Chapter 9
Induced polarisation

9.1 INTRODUCTION

The phenomenon of *induced polarisation* (IP) is reported to have been noted by Conrad Schlumberger as early as 1912. The induced polarisation method has been used since the late 1940s, having been developed during the Second World War by William Keck and David Bliel as part of a US Navy project to detect mines at sea (Grow 1982). One aspect of IP, known as the *overvoltage effect*, has been known about since the nineteenth century.

In the 1980s there were considerable advances in instrumentation, and sophisticated techniques such as *complex resistivity* and *spectral IP* (Pelton *et al.* 1978) were developed, although there is still much research to be done to relate geological causes to the observed

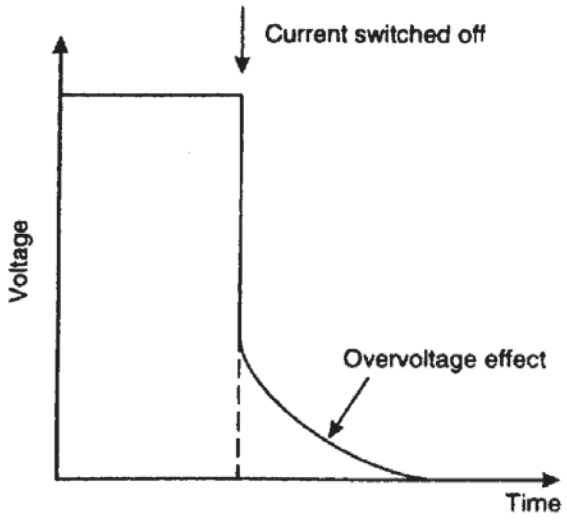

Figure 9.1 The overvoltage effect produced by induced polarisation after an applied current is switched off

geophysical data. Thus, there are difficulties in attempting quantitative interpretation.

The main current application of IP prospecting is in the search for disseminated metallic ores and, to a lesser extent, groundwater and geothermal exploration. Since the early 1990s, there has been an increased interest in the possible use of IP methods in environmental applications, although the work is still very much at a research stage.

Measurements of induced polarisation are made using conventional electrical resistivity electrode configurations (see Chapter 7) involving two current and two non-polarisable potential electrodes. When the applied current is switched off, the voltage between the potential electrodes takes a finite and measurable time (seconds to several minutes) to decay to zero (Figure 9.1) because the ground temporarily stores charge (i.e. becomes polarised) and acts somewhat like a capacitor. When the current is switched back on, the voltage does not peak instantaneously but builds up over the same time period (the *rise-time*) to its maximum applied value. The voltage decay and rise-time are dependent upon both instrumental and geological factors, and are thus diagnostic of the nature of the ground, as will be discussed later.

There are four systems of induced polarisation measurement. *Time domain* (or *pulse transient*) techniques measure the overvoltage as a function of time; and in *frequency domain* methods the apparent resistivity is measured at two or more different frequencies (usually lower than 10 Hz–Patella and Schiavone 1977). In the *phase domain* technique, the phase-lag between the applied current and the measured voltage is diagnostic of the nature of the sub-surface mineralisation. In *spectral IP*, phase and magnitude are measured over a range of frequencies from 10^{-3} to 4×10^{3} Hz.

The induced polarisation method is an active one because voltages, which can be as high as several thousand volts in time-domain surveys, are applied to the ground in order to generate measurable overvoltages. The equipment used is similar to, but much more elaborate than, that employed in electrical resistivity work. The induced polarisation method excites (induces) a response in the ground which is dependent upon the distribution and nature of mineral grains present, and is most effective when the mineral grains are disseminated rather than combined in a massive form, as explained in the next section.

9.2 ORIGIN OF INDUCED POLARISATION EFFECTS

The exact causes of induced polarisation phenomena are still unclear, but the two main mechanisms that are reasonably understood are *grain (electrode) polarisation (overvoltage)* and *membrane (electrolytic) polarisation*, both of which occur through electrochemical processes.

9.2.1 Grain (electrode) polarisation

Grain or electrode polarisation occurs by the same process that results in self-potentials (see Chapter 8). If a metal electrode is placed in an ionic solution without a voltage being applied, charges with different polarities separate, resulting in the establishment of a potential difference between the electrode and the solution (Figure 9.2). The total magnitude of the potential is the Nernst potential and the adsorbed layer gives rise to the zeta potential (see Section 8.3.2). When a voltage is applied, the ionic balance is disturbed; this causes a current to flow, which in turn changes the potential difference between the electrode and the solution. When the applied voltage is removed, the ionic balance is restored by the diffusion of ions.

In the geological situation, current is conducted through the rock mass by the movement of ions, within groundwater, passing through interconnected pores or through the fracture and micro-crack structure within the rock. When an electronically conducting grain (e.g. a metal sulphide) blocks a flow channel, charge builds up (Figure 9.3) as in the electrochemical cell; this opposes the current flow and the grain becomes polarised, so creating a potential difference across the grain. On switching off the applied voltage, the ions diffuse back through the electrolytic medium and the potential difference acrosss the grain reduces to zero in a finite time, giving the characteristic overvoltage decay measured in time-domain systems.

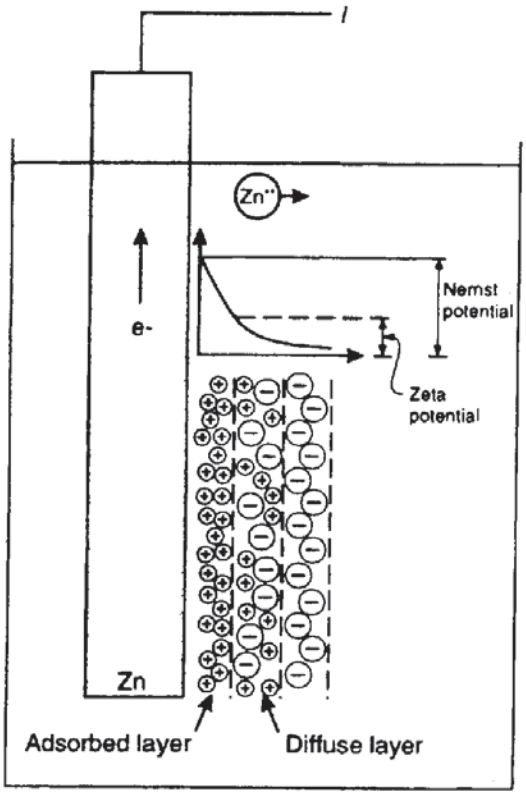

Figure 9.2 The phenomenon of electrode polarisation with the physical processes by which the Nernst and zeta potentials are obtained. From Beck (1981), by permission

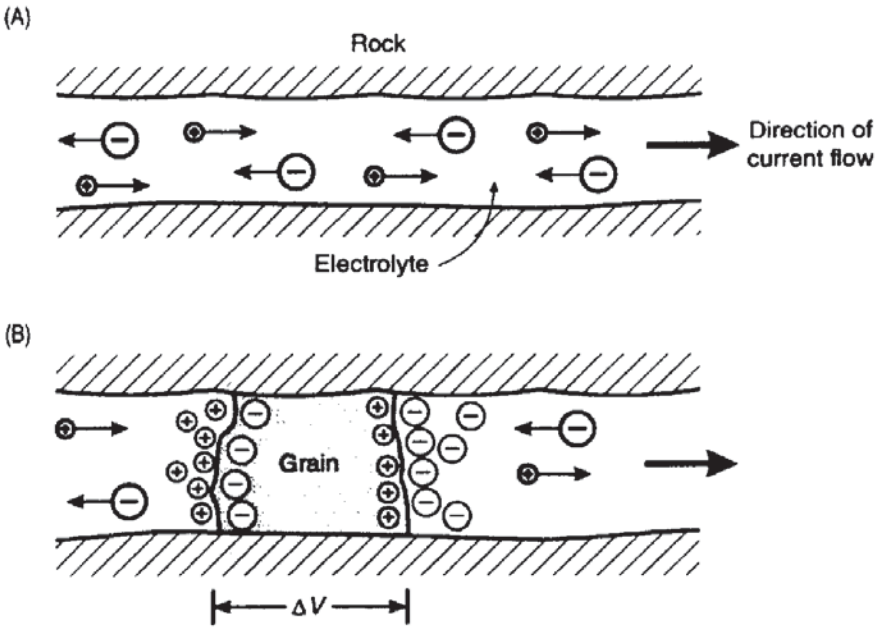

Figure 9.3 Grain (electrode) polarisation. (A) Unrestricted electrolytic flow in an open channel. (B) Polarisation of an electronically conductive grain, blocking a channel

Grain polarisation is essentially a surface phenomenon and this is why *disseminated* ores (with correspondingly large total surface areas) produce a significant IP response. (Sometimes an IP response is obtained over a halo of disseminated ore around a massive orebody.) Although it is the individual electronically conducting mineral grains

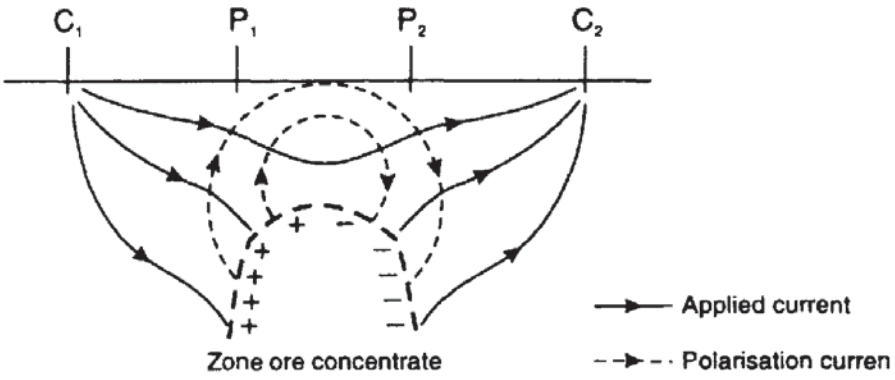

Figure 9.4 Macroscopic effect c grain polarisation over a disseminate ore body

that become polarised, complete zones with significant concentrations of ore will also take on a net polarisation; this results in a macroscopic polarisation current flow in the ground which is measured as the IP response. For the Wenner electrode configuration (see Section 7.3.2) in Figure 9.4, current polarises the zone of ore concentration which, when the applied current is turned off, generates the transient polarisation current that is measured at the surface. The current field is more complicated for the more commonly used dipole–dipole electrode array (see Section 7.3.2). The factors affecting the rate at which the ionic balance is restored are extremely complex and may depend upon the pore shape and size, rock structure, permeability, electrolytic conductivity and ionic concentration, and on the electronic conductivity of the mineral grain. Bornite, cassiterite, chalcopyrite, galena, graphite, limenite, magnetite, pyrite, pyrolusite and pyrrhotite, all exhibit strong IP responses as they have high electronic conductivities. The sulphides sphalerite, cinnabar and stibnite have low electronic conductivities and do not produce significant IP responses. For the same reason, they tend to produce only minimal, if any, self-potentials.

9.2.2 Membrane (electrolytic) polarisation

An IP response measured over rocks that do not contain sulphide mineral grains can be indistinguishable from the IP overvoltage effect over rocks containing low concentrations of disseminated ores, especially if traditional methods of time- and frequency-domain measurement are used. However, the more modern spectral and phase-domain IP systems may provide sufficiently diagnostic results.

There are two causes of membrane or electrolytic polarisation. One is by the constriction within a pore channel and the other is associated with the presence of clay within pore channels, such as in an impure sandstone. There is a net negative charge at the interface between most rock minerals and pore fluids. Positive charges within the pore

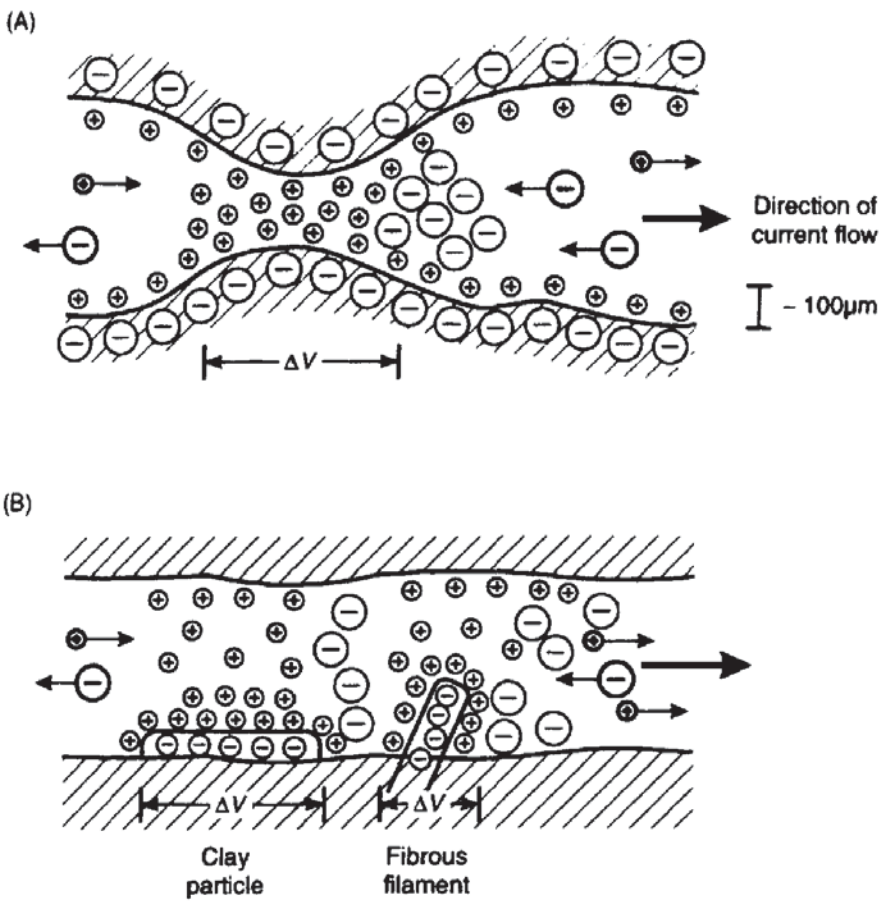

Figure 9.5 Development of membrane polarisation associated with (A) a constriction within a channel between mineral grains, and (B) negatively charged clay particles (Fraser *et al.* 1964) and fibrous elements along the sides of a channel

fluid are attracted to the rock surface and build up a positively charged layer up to about 100 μm thick, while negative charges are repelled. Should the pore channel diameter reduce to less than this distance, the constriction will block the flow of ions when a voltage is applied. Negative ions will leave the constricted zone and positive ions will increase their concentration, so producing a potential difference across the blockage (Figure 9.5A). When the applied voltage is switched off, the imbalance in ionic concentration is returned to normal by diffusion, which produces the measured IP response.

The second cause of membrane polarisation is the presence of clay particles or filaments of fibrous minerals, both of which tend to have a net negative charge. Positive ions are attracted to them, producing a positively charged cloud within the pore space. When a voltage is applied, positive charges can move between these similarly charged clouds but the negatively charged ions are blocked, which produces a difference in ionic concentration (Figure 9.5B). When the applied voltage is switched off, the imbalances in ionic concentration decay to normal levels by diffusion, so causing a measurable IP response.

9.2.3 Macroscopic processes

Various attempts have been made to explain induced polarisation in a quantitative way (e.g. Bertin and Loeb 1976) and to describe the phenomena qualitatively (e.g. Shuey and Johnson 1973; Sumner 1976). It is vital for interpretational purposes that any hypothesis should be able to explain the shape of the overvoltage decay curve with time and the variation of resistivity and phase with frequency. Indeed, the time-decay curve behaves in a complex manner proportionately to t^{-n}, where t is the time since the current was turned off – rather than being an exponential decay. Arguments involve the current density within and the dielectric constant (see Chapter 10) of the geologic material, but the induced polarisation phenomenon cannot be explained simply in terms of the dielectric constant of the rock. Models, which tend to be two-dimensional, fail to account adequately for three-dimensional reality, although Hohmann (1975) has attempted 3-D modelling. Some models have succeeded in identifying electric-circuit analogues in terms of resistor–capacitor systems (Bertin and Loeb 1976), but these are not explanations of the *physical* processes within the ground which give rise to induced polarisation.

9.2.4 Ionic processes

Just as macroscopic theories have failed to provide an adequate solution, so too have those that consider processes on the microscopic level. Forces acting on the ions and their resultant motions have been considered under diffusion theory which dates back to the end of the last century. The amplitude of the overvoltage in time-domain measurements should change as the square-root of the frequency but, according to experiments, it does not. If electrical forces are considered in addition to general diffusion, which takes into account the electric field and the ionic mobility, then it is possible to obtain dielectric parameters which are much closer to those derived from actual measurements. The effect of thermal agitation has also been considered and consequent mathematical modelling does reproduce the time-dependence of the overvoltage decay. Satisfactory physical explanations have yet to be found (Schufle 1958; Wong 1979).

9.3 MEASUREMENT OF INDUCED POLARISATION

Current is applied to the ground by means of two current electrodes, and the induced-polarisation effect is measured between two potential electrodes, most commonly in a dipole–dipole array. Some-

times Wenner, Schlumberger (gradient) and pole–dipole arrays are used. (For electrode array types, see Section 7.3.2.) Subsequent discussion of this method will be based on the use of the dipole–dipole array.

Electrode spacings are commonly tens to several hundred metres, but in broad reconnaissance surveys – for which the Schlumberger array tends to be used – the spacings can be even larger. The type of equipment used is bulkier and more elaborate than that used for resistivity surveys, and also depends on the type of IP survey being conducted. A transmitter is used to generate the applied current input into the ground, and the polarisation effects are detected by a receiver comprising non-polarisable porous-pots connected to the potential electrodes (see Chapter 8). Profiles are undertaken with fixed electrode spacings in much the same way as in the constant-separation traversing of electrical resistivity surveys (Chapter 7). More details of the field arrangements are given by Telford *et al.* (1990) and Milsom (1989).

9.3.1 Time-domain measurements

When a current is applied to the ground and switched off a few moments later, an overvoltage decay results (Figure 9.6). The total magnitude of the observed voltage (V_O) is equal to the actual voltage (V) due to the applied current plus a polarisation voltage (V_P) caused by the polarisation processes (Section 9.2). When the applied current is switched off, the voltage drops instantaneously by the amount V, leaving a residual voltage (the overvoltage) (V_P) which decays with time. One measure of the IP effect is the ratio V_P/V_O which is known as the *Chargeability* and is usually expressed in terms of millivolts per volt or per cent.

Instrumentally, it is extremely difficult to measure V_P at the moment the current is switched off, so it is measured at a fixed time (typically 0.5 s) after cutoff. Measurements are then made of the decay of V_P over a very short time period (0.1 s) after discrete intervals of time (also around 0.5 s). The integration of these values with respect to time gives the area under the curve (Figure 9.6), which is an alternative way of defining the decay curve. When the integral is divided by V_O, the resultant value is called the *apparent chargeability* (M_a) and has units of time (milliseconds) (see Box 9.1).

The *true* chargeability is virtually impossible to measure in a field situation as each layer within the ground will have its own absolute value of chargeability and of true resistivity. What is measured is a complex function of all the true resistivities and absolute chargeabilities for all the media being sampled within the range of the equipment. A short charging period will produce a lower IP response than a long charging period (Figure 9.7).

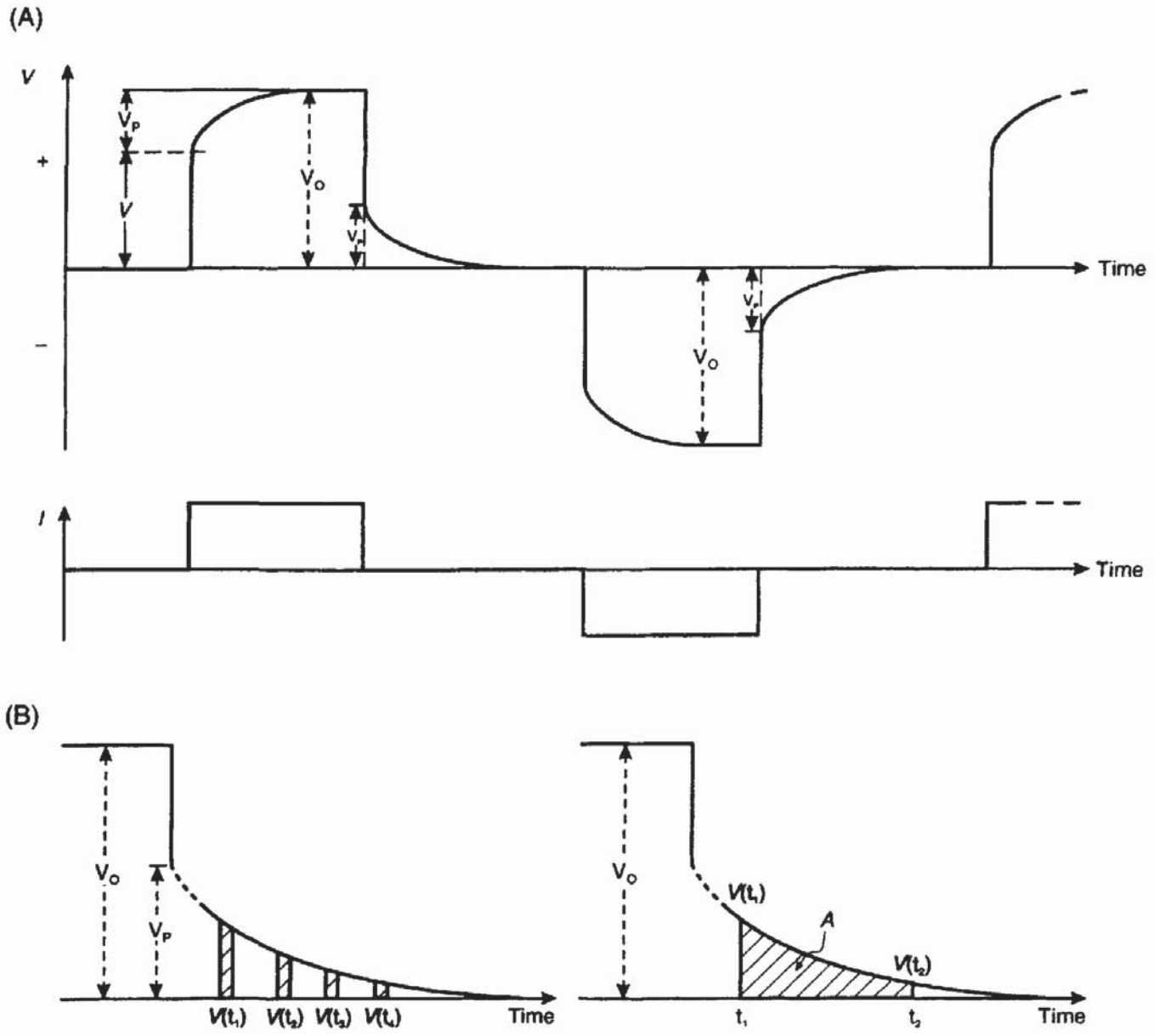

For given charging and integration periods (which differ between makes of IP equipment), the measured apparent chargeability is a diagnostic parameter that can be interpreted qualitatively in terms of the sub-surface geology. For a charging time of 3 s, an integration period of 1 s and a 1% volume concentration, chalcocite has a value of M_a of 13.2 ms, which is more than twice that of bornite (6.3 ms) and slightly higher than that of graphite (11.2 ms). In contrast, magnetite has a value of only 2.2 ms, and hematite has zero apparent chargeability.

Figure 9.6 (A) Application of a pulsed current with alternate polarity, and the consequent measured voltage showing the effect of the overvoltage (V_P) and the rise-time on the leading edge of the voltage pulse. (B) Two forms of measurement of the overvoltage at discrete time intervals $V(t_1)$, etc., and by the area beneath the overvoltage curve (A)

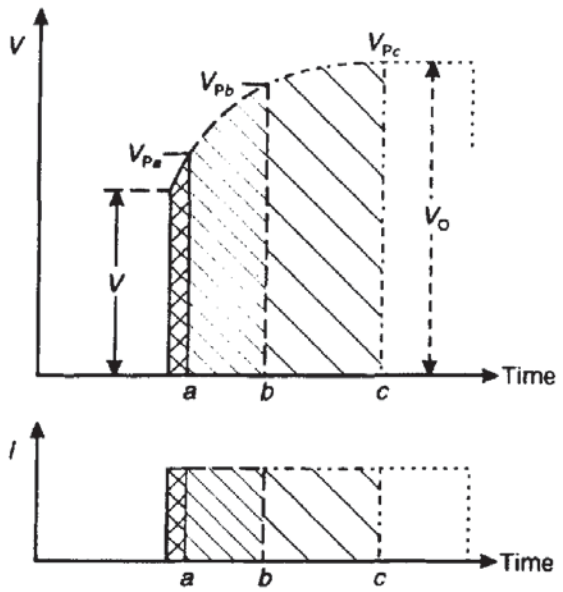

Figure 9.7 Increasing the charging time (*a* to *c*), which decreases the frequency of measurement, has the effect of increasing the overvoltage (V_{Pa} to V_{Pc}). Consequently, the apparent resistivity at lower frequency (e.g. at *c*) is greater than that at a higher frequency (e.g. at *a*)

Box 9.1 Chargeability (see Figure 9.6)

Chargeability:

$$M = V_P/V_O \text{ (mV/V or \%)}$$

where V_P is the overvoltage, and V_O the observed voltage with an applied current.

Apparent chargeability:

$$M_a = \frac{1}{V_O}\int_{t_1}^{t_2} V_P(t)\,dt = \frac{A}{V_O}$$

where $V_P(t)$ is the overvoltage at time t, and the other terms are as defined in Figure 9.6B.

The major advantage of integration and normalising by dividing by V is that noise from cross-coupling of cables and from background potentials is reduced. Care has to be exercised in selecting appropriate time intervals to maximise signal-to-noise ratios without reducing the method's diagnostic sensitivity.

9.3.2 Frequency-domain measurements

In frequency-domain (variable frequency) induced-polarisation studies, the apparent resistivity is measured at two frequencies less than 10 Hz (e.g. 0.1 and 5 Hz, or 0.3 and 2.5 Hz) using the same electrode array as in time-domain and direct-current resistivity measurements. The apparent resistivity at low frequency (ρ_{a0}) is greater than that at a higher frequency (ρ_{a1}) for reasons which can be appreciated by

reference to Figure 9.7. For a short charging time the measured overvoltage is appreciably lower (V_{Pa}) than that obtained for longer charging times (V_{Pb} and V_{Pc}).

The length of the decay is too short to be determined, so the total amplitude of voltage is measured with respect to the applied current, giving a value of the resistance (R) which, when multiplied by the appropriate geometric factor (see Section 7.3.2), is the apparent resistivity. If the current is switched in polarity, and on and off, with a time delay comparable to the length of the charging time, then this is the same as applying an alternating current signal at a given frequency (f hertz). The shorter the charging and delay times, the higher the frequency, and so the apparent resistivity at low frequency is greater than that at a higher frequency. The two apparent resistivities are used to determine the *frequency effect* (FE) (unitless), which can be expressed alternatively as the *percentage frequency effect* (PFE) (units: %) (Box 9.2).

Box 9.2 Frequency effect (*FE*)

Frequency effect:

$$FE = (\rho_{a0} - \rho_{a1})/\rho_{a1} \text{ (unitless)}$$

where ρ_{a0} and ρ_{a1} are the apparent resistivities at low and higher frequencies respectively, and $\rho_{a0} > \rho_{a1}$.

Percentage frequency effect:

$$PFE = 100\,(\rho_{a0} - \rho_{a1})/\rho_{a1} = 100\,FE.$$

The frequency effect in the frequency-domain is equivalent to the chargeability in the time-domain for a weakly polarisable medium where FE is very much less than 1.

Marshall and Madden (1959) modified the expression involving the frequency effect to produce the *metal factor* (MF) (or the *metal conduction factor*) (Box 9.3). It is thought by some geophysicists that metal factor data delineate disseminated sulphide zones more effectively than frequency effect data.

Box 9.3 Metal factor (*MF*)

Metal factor:

$$MF = A(\rho_{a0} - \rho_{a1})/(\rho_{a0}\rho_{a1}) \text{ (units: siemens/m)}$$
$$= A(\sigma_{a1} - \sigma_{a0})$$

where ρ_{a0} and ρ_{a1} are the apparent resistivities, and σ_{a0} and σ_{a1} are the apparent conductivities ($= 1/\rho_a$) at low and higher frequencies respectively; $\rho_{a0} > \rho_{a1}$ and $\sigma_{a0} < \sigma_{a1}$; and $A = 2\pi \times 10^5$.

continued

continued

Alternatively, the metal factor is given by:

$$MF = A \times FE/\rho_{a0} = A \times FE/\rho_{a0} = FE/\rho_{a0} = A \times FE \times \sigma_{a0}$$

where FE is the frequency effect.

Although disseminated orebodies can be located using IP data, chargeability, frequency effect and metal factor do not give a good indication of the relative amount of the metallic mineralisation within the source of the IP response. It is necessary to go to more elaborate methods such as spectral IP, and even then the estimates obtained are not unambiguous.

(One further frequency-domain method that has been used but which has been superseded by the spectral IP method is 'phase IP'. Only one frequency is necessary. Induced polarisation is identified by the presence of a phase lag (ϕ) between the applied current and the polarisation voltage measured.)

9.3.3 Spectral IP and complex resistivity

Spectral IP is another name for complex resistivity, which in turn is related to the measurement of the dielectric properties of materials. An overview of the theoretical basis and interpretation of spectral IP (complex resistivity) data is given by Pelton *et al.* (1983).

The same field arrangement is used as in time- and traditional variable-frequency surveys but the equipment is considerably more sophisticated. It is important that the measurements be as precise as possible and that any noise be eradicated (see next section).

The magnitude of the complex resistivity ($|Z(\omega)|$) and phase (ϕ) of the polarisation voltage are measured over a wide range of frequencies (0.3 to 4 kHz) of applied current, which results in a diagnostic IP response spectrum (Figure 9.8). The frequency dependence is usually plotted as a binary function in the form of logarithms to base 2 rather than to base 10. The behaviour between the lower and upper frequency limits is known as the 'relaxation' of the electrical system (Shuey and Johnson 1973) and the entire dispersion can be defined if four electrical parameters are known (Box 9.4), namely, the DC resistivity (ρ_0), the IP chargeability (M), the time constant of the IP response (τ; also known as the relaxation time in dielectric studies), and the exponent of the angular frequency (ω).

Box 9.4 Spectral IP response

$$|Z(\omega)| = \rho_0\left[1 - M\left(1 - \frac{1}{1 + (i\omega\tau)^c}\right)\right]$$

where ρ_0 is the DC resistivity, M is the IP chargeability, ω is the angular frequency, τ is the time constant, and $i = \sqrt{-1}$.

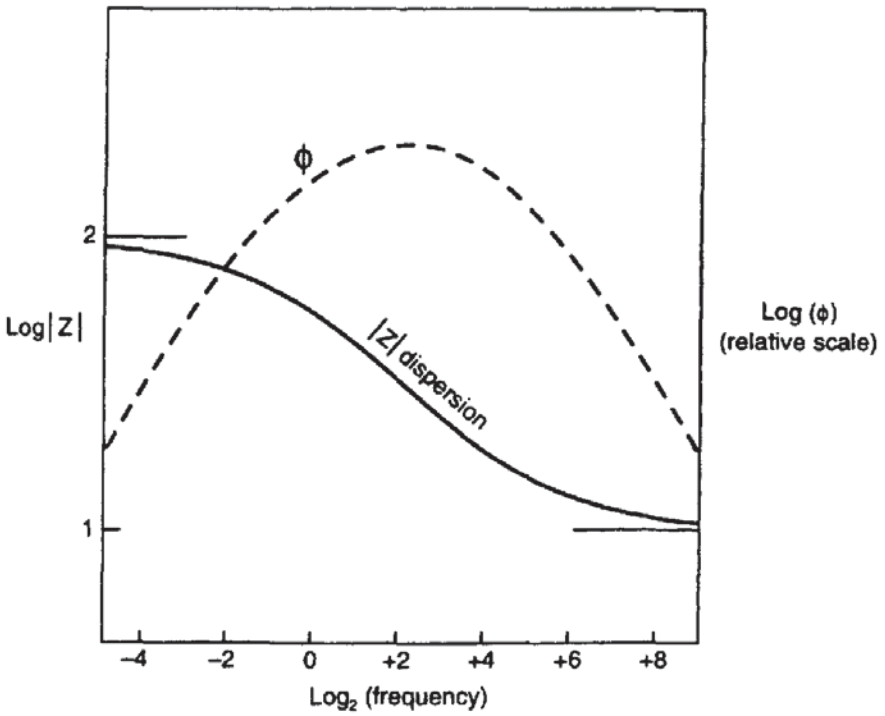

Figure 9.8 A typical IP spectral response (Pelton *et al.* 1983)

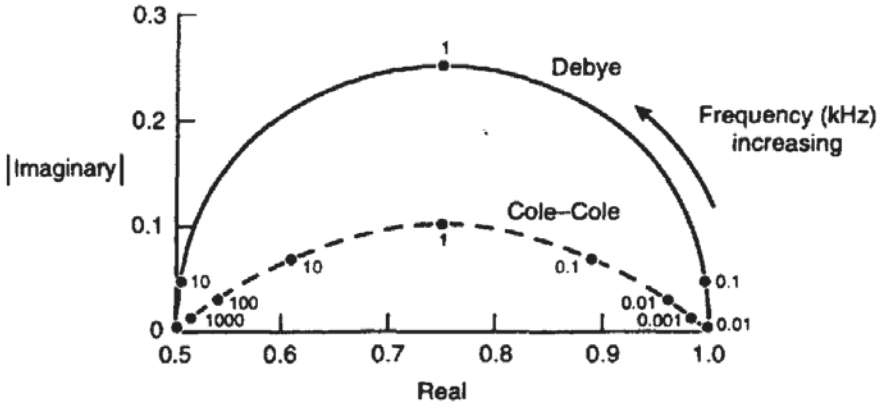

Figure 9.9 Cole–Cole relaxation spectra for Debye and Cole–Cole dispersions for $\tau = 1/2\pi$ and $c = 0.5$ (Pelton *et al.* 1983)

One form of relaxation commonly used is the *Cole–Cole relaxation spectrum* (Figure 9.9), named after its originators Cole and Cole (1941). This can be characterised by the critical frequency (F_c) which is the specific frequency at which the maximum phase shift is measured (Box 9.5). Note that this frequency is completely independent of resistivity. Phase angle and the critical frequency increase with increasing chargeability (Figure 9.10).

Box 9.5 Critical frequency (F_c)

$$F_c = [2\pi\tau(1 - M)^{1/2c}]^{-1}$$

where τ is the time constant, and M the IP chargeability.

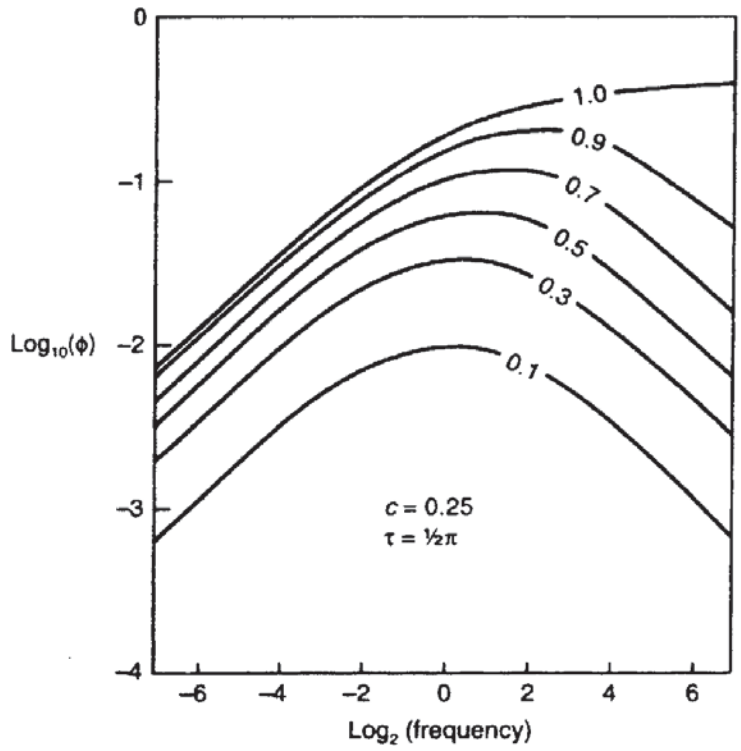

Figure 9.10 Phase angle curves for a typical Cole–Cole model with different chargeability ($M = 0.1$–1.0) (Pelton *et al.* 1983)

The fitting of two or more Cole–Cole dispersions to field spectra, a process known as *SIP inversion* (Song and Vozoff 1985), is the means by which the various intrinsic dielectric parameters are obtained. The 'texture' of mineralisation, which is characterised by the grain size and grain-size distribution of the polarisable particles within each group of ore grains but which is less dependent on the type of metallic minerals present, dictates the behaviour of the time constant (τ) and the frequency exponent (c). Where the polarisable mineralisation is coarse-grained, the relaxation time (τ) is large and the critical frequency (F_c) is small (conversely for fine-grained mineralisation). Similarly, massive sulphide orebodies have a distinctly different chargeability–relaxation time behaviour compared with graphite (Hallof and Klein 1982), and magnetite has a distinct chargeability–relaxation time behaviour compared with that of pyrrhotite (Pelton *et al.* 1978) (Figure 9.11). The maximum value of c is 0.5, and for most massive sulphides c is in the range 0.25–0.35 (Hallof 1983). Examples of the phase behaviour for several cases with various grain-size populations are illustrated in Figure 9.12. Where two grain-size distributions overlap or where a wide range of grain-sizes is distributed continuously, values of c fall to between 0.1 and 0.2 and the spectral curve is very flat. Computer analysis of such flat spectral curves is insensitive to variations in both c and τ and the estimations of grain-size distributions are likely to be ambiguous. Phase-angle spectra associated with different types of orebody are shown in

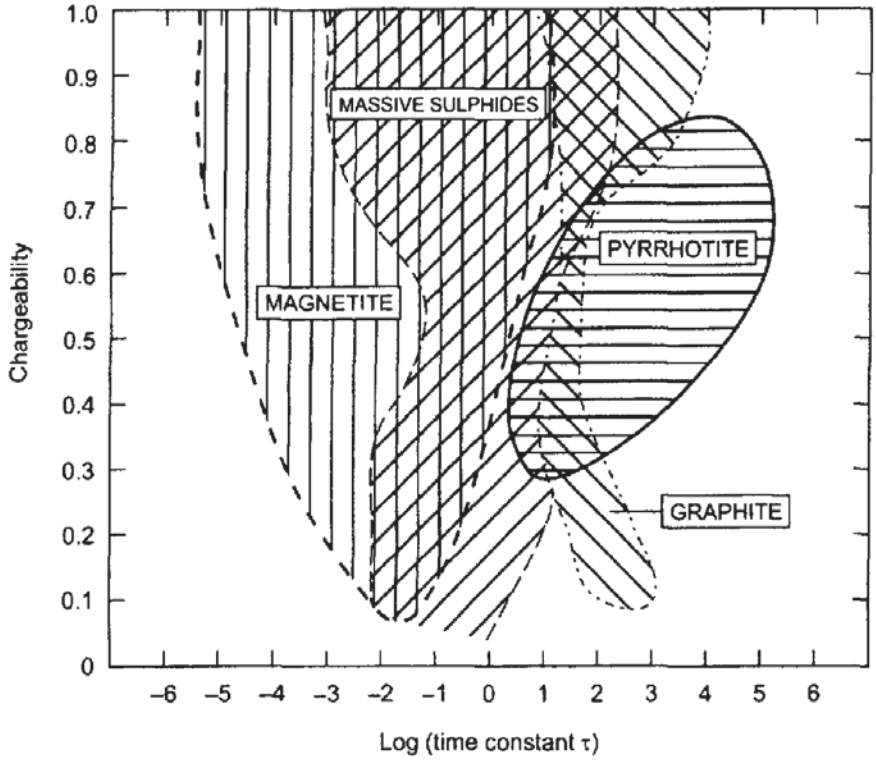

Figure 9.11 Chargeability as a function of relaxation time constant τ. After Hallof and Klein (1992), and Pelton *et al.* (1978), by permission

Figure 9.13. If chargeability–τ data plot in an overlapping field (such as magnetite and massive sulphides in Figure 9.11), then the phase-angle spectrum can be used to differentiate between the two ore types (Pelton *et al.* 1978).

Spectral IP parameters can be used to determine the mineralisation texture of an orebody and so separate out zones of primary mineralisation which consist of veinlets of ore from those of disseminated ore. Where long zones of sulphide or oxide iron formations occur, spectral IP can indicate where base metal concentrations increase by variations in the spectral 'texture'. In addition, changes in 'texture' along a pyrite zone may indicate the presence of gold, copper or zinc compared with barren areas (Hallof 1983).

The interpretation of spectral IP remains limited by the continued lack of understanding of the dielectric properties of rocks. The behaviour of the various dielectric parameters, such as the relaxation time, may vary with different physical conditions, such as with temperature (Saint-Amant and Strangway 1970; Ogilvy and Kuzmina 1972; Reynolds 1985). Assuming that dielectric parameters behave isothermally may result in misleading interpretations. One example of where this temperature dependence may be of practical advantage has been given by Reynolds (1985, 1987b). The relaxation time for glacier ice is strongly temperature-dependent. Temperate

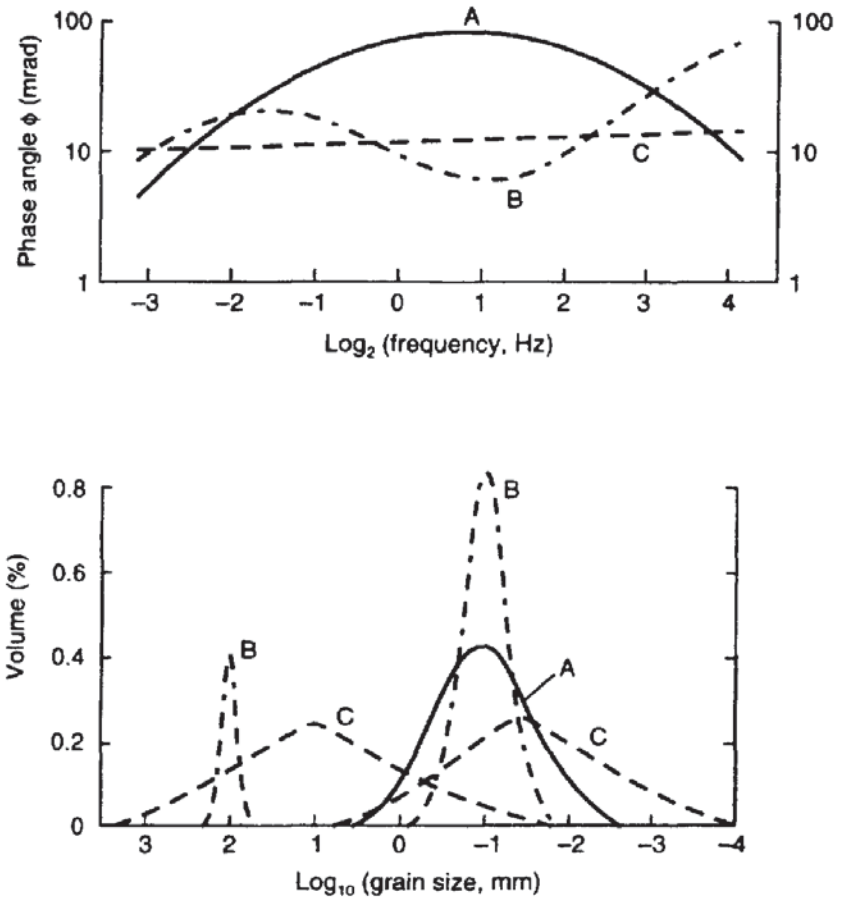

Figure 9.12 Theoretical spectral plots of phase with three models of grain size distributions. Data from Hallof (1983), by permission

glacier ice (i.e. ice at its pressure melting point throughout) has a diagnostically different temperature-dependence of relaxation time compared with that for polar glacier ice (i.e. ice well below its pressure melting point) (Figure 9.14). Some glaciers have both temperate and polar ice zones, with important implications for glacier ice flow and hazard evaluation, which can be differentiated by the dielectric measurement of relaxation time of ice samples. Spectral IP measurements have yet to be made over glaciers but the information obtained should prove to be immensely useful glaciologically. Spectral IP could also have applications in mapping out and distinguishing between massive ice bodies and interstitial ice in permafrost.

9.3.4 Noise reduction and electromagnetic coupling

To attain the high level of accuracy required for spectral IP, noise and electrical distortion of the IP response must be minimised before interpretation can proceed. There are four types of extraneous signal, of which three (current electrode variations, self-potentials and telluric currents) are regarded as 'noise' in IP work, and the remaining one

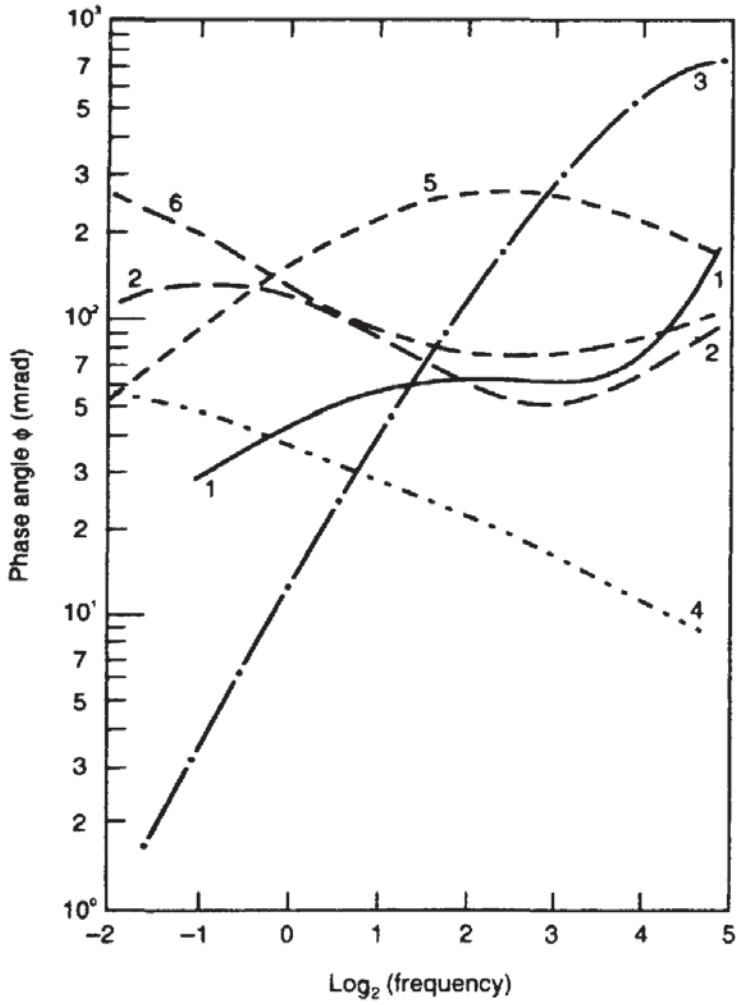

Figure 9.13 Characteristic phase-angle plots for different types of mineralisation. Data from Pelton *et al.* (1978), by permission

(electromagnetic inductive coupling) is a distortion that occurs at higher frequencies and has to be estimated and removed from the data (Hallof 1974; Hallof and Pelton 1980).

The noise signals can be constrained within the instrument by the use of filters. Current electrode variations due to changing current flow and the frequency of the applied current cause distortions within the waveform of the applied current. To compensate for this, a multi-channel approach is taken to measure voltage. Up to six pairs of potential electrodes are used to measure the IP voltage simultaneously, and the waveform of each pair is compared directly with that of the applied current so that the exact magnitude and phase of the signal waveform can be obtained for each of the six channels.

The most problematical effect is that due to electromagnetic coupling which occurs particularly at large electrode separations and at higher frequencies. The highest frequencies used in IP work overlap with the lower frequencies used by electromagnetic prospecting methods where *induction* becomes important. If a wire carrying

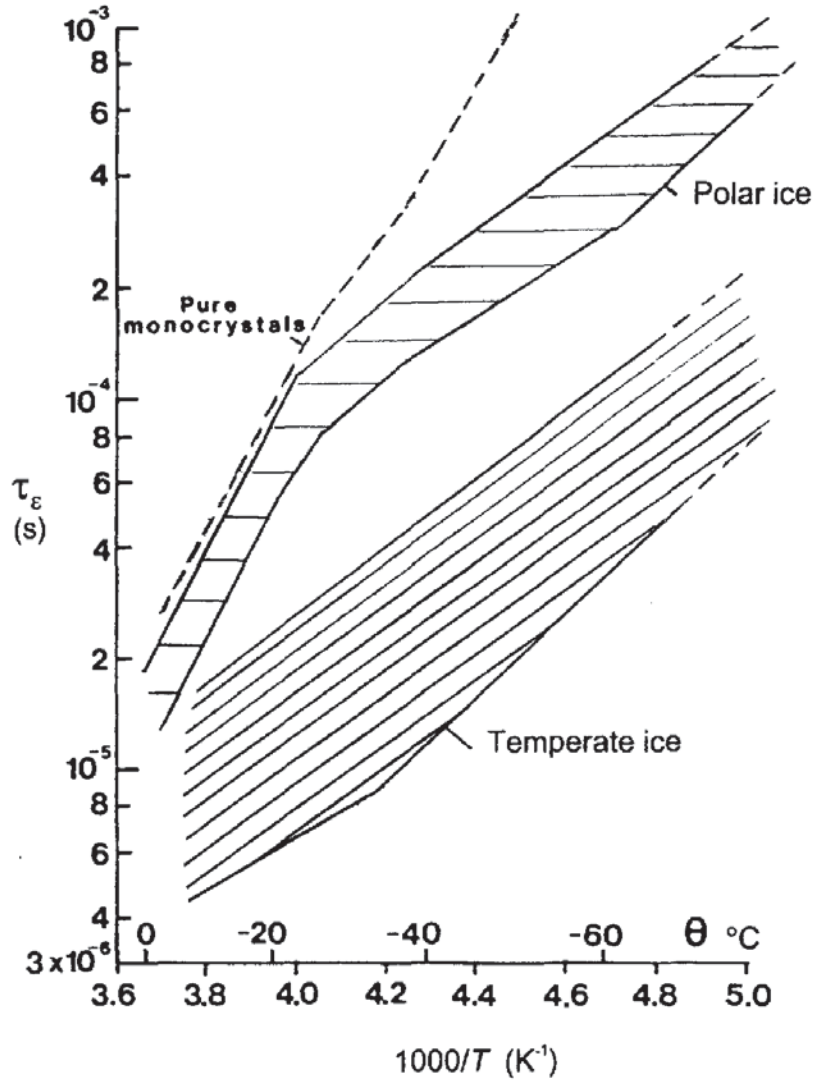

Figure 9.14 Temperature dependence of relaxation time constant τ for temperate and polar glacier ice, illustrating that τ can be used to differentiate between the thermal regimes of the two ice types. After Reynolds (1985), by permission

a current lies close to and parallel to another wire, a current will be induced into the second wire, such as happens close to power grid cables. If this induction occurs in wires connected to potential electrodes, spurious voltages will be measured. It is best to keep current-carrying cables well away from potential cables or to ensure that the two types of cable cross each other at right-angles. Furthermore, the current-carrying cables can induce a current into the ground which will distort the IP response. Fortunately, the frequency dependence of the electromagnetic coupling is recognisably different from that of the IP response and, if high enough frequencies are used, the coupling effects can be measured and then determined for the whole frequency range and removed from the data (Hohmann 1973; Wynn and Zonge 1975; Sumner 1976; Rathor 1977; Pelton *et al.* 1978; Hallof 1983). Pipelines have also been recognised as contributing to noise in IP surveys (Parra 1984).

9.3.5 Forms of display of IP data

Induced polarisation data for a given electrode separation, particularly when measured in the time domain, are commonly plotted as simple profiles and maps of chargeability (see Figure 8.6), metal factor or percentage frequency effect. In frequency-domain methods it is more usual to plot the data in the form of a pseudo-section (Figure 9.15).

Note that the spacing of the data points is dependent upon the integer value of n in dipole–dipole arrays and not on the actual dipole length. However, the increasing depth of penetration is implicit in the larger values of n and, as a guide, the depth of penetration is approximately equal to $a/2$ for $n = 2$; $\approx a$ for $n = 3$; and $\approx 2a$ for $n = 4$, where a is the dipole length. Each data value is plotted at the intersection of two lines drawn at 45° to the midpoint of each dipole used in the measurement. Two positions are indicated, for example, in Figure 9.15. For $n = 1$, and dipoles 1–2 and 3–4, the measured data

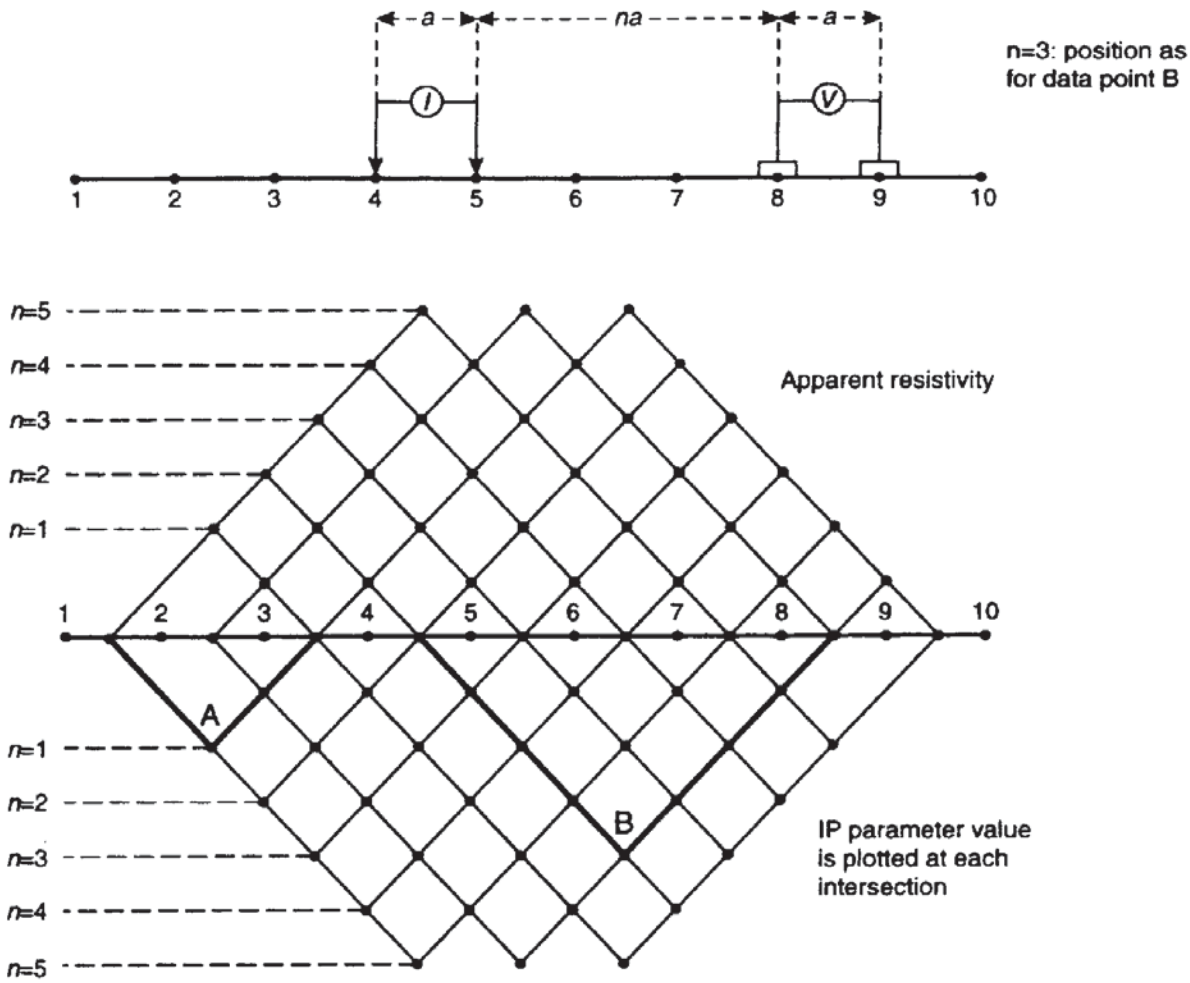

Figure 9.15 How to plot a pseudo-section. For a dipole–dipole array with current and potential electrodes at 1–2 and 3–4 respectively ($n = 1$), the measuring point is plotted at A; for dipoles at 4–5 and 8–9 ($n = 3$), the data value is plotted at B

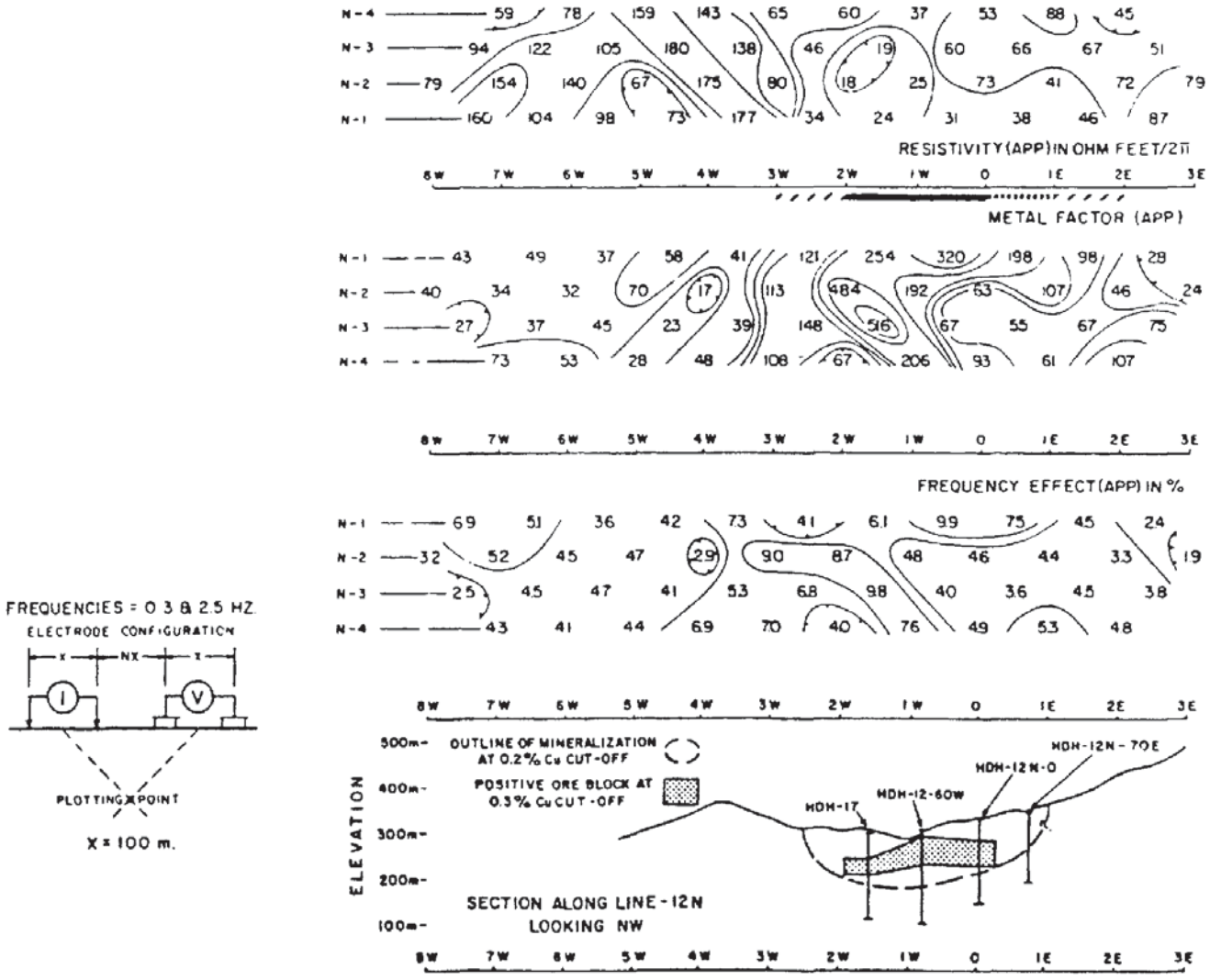

value is plotted at A; for $n = 3$ and dipoles 4–5 and 8–9, the position is at B. It is usual for the apparent resistivity pseudo-section to be drawn inverted above those for other IP parameters. Apparent resistivity, which is often plotted in units of $\Omega\,m/2\pi$, can also be plotted the correct way up as convenient. The plotted values can then be contoured. The surface projection of zones with IP anomalies are indicated respectively by solid, dashed, or oblique dashed bars along the top of the pseudo-section to indicate the location of definite, probable and possible mineralisation (Figure 9.16).

The interpretation of such displays tends to be by qualitative comparison with those obtained for theoretical or experimental scale models. Examples of the apparent resistivity, apparent metal factor and apparent phase for two models are given in Figure 9.17. In both cases the patterns in all three IP parameters are symmetrical about the central position and form patterns in the form of an inverted V.

Figure 9.16 Apparent resistivity, metal factor and frequency effect profiles over the Hinobaan deposit whose geological cross-section is shown schematically in the lower diagram. A dipole length of 100 m and frequencies of 0.3 and 2.5 Hz were used. From Pelton and Smith (1976), by permission

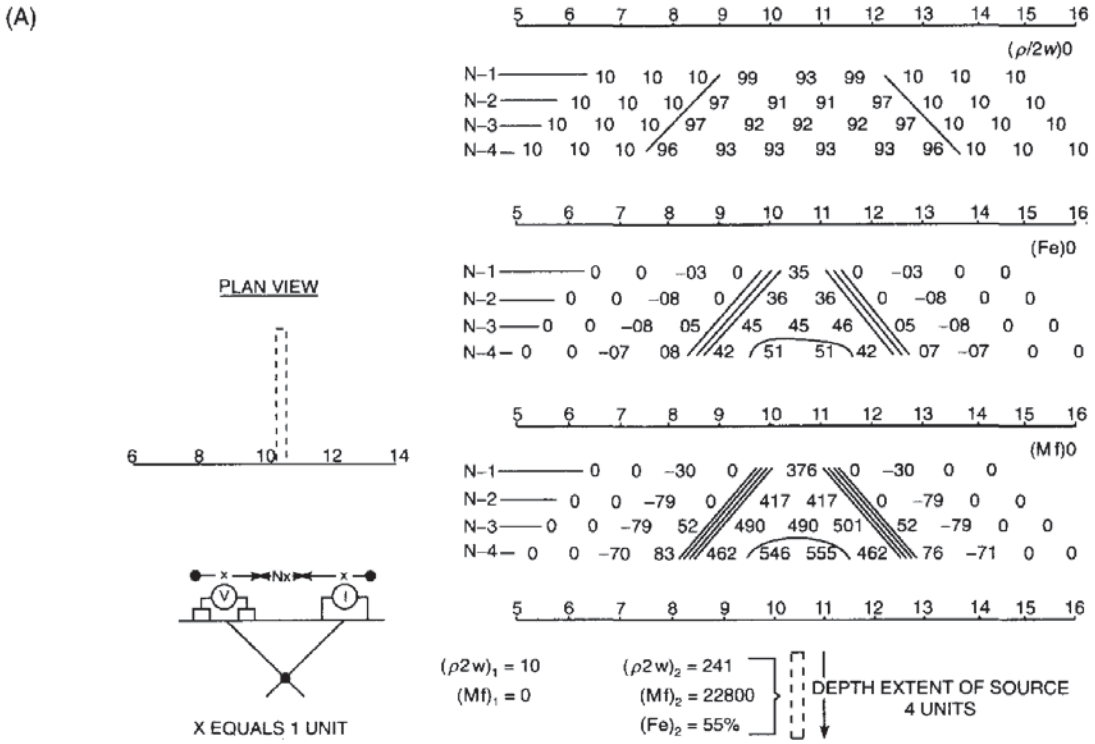
(A)
5 6 7 8 9 10 11 12 13 14 15 16
(ρ/2w)0
N–1 10 10 10 99 93 99 10 10 10
N–2 10 10 10 97 91 91 97 10 10 10
N–3 10 10 10 97 92 92 92 97 10 10 10
N–4 10 10 10 96 93 93 93 93 96 10 10 10
(Fe)0
N–1 0 0 –03 0 35 0 –03 0 0
N–2 0 0 –08 0 36 36 0 –08 0 0
N–3 0 0 –08 05 45 45 46 05 –08 0 0
N–4 0 0 –07 08 42 51 51 42 07 –07 0 0
(Mf)0
N–1 0 0 –30 0 376 0 –30 0 0
N–2 0 0 –79 0 417 417 0 –79 0 0
N–3 0 0 –79 52 490 490 501 52 –79 0 0
N–4 0 0 –70 83 462 546 555 462 76 –71 0 0
PLAN VIEW
6 8 10 12 14
x Nx x
V I
X EQUALS 1 UNIT
(ρ2w)1 = 10
(Mf)1 = 0
(ρ2w)2 = 241
(Mf)2 = 22800
(Fe)2 = 55%
DEPTH EXTENT OF SOURCE
4 UNITS

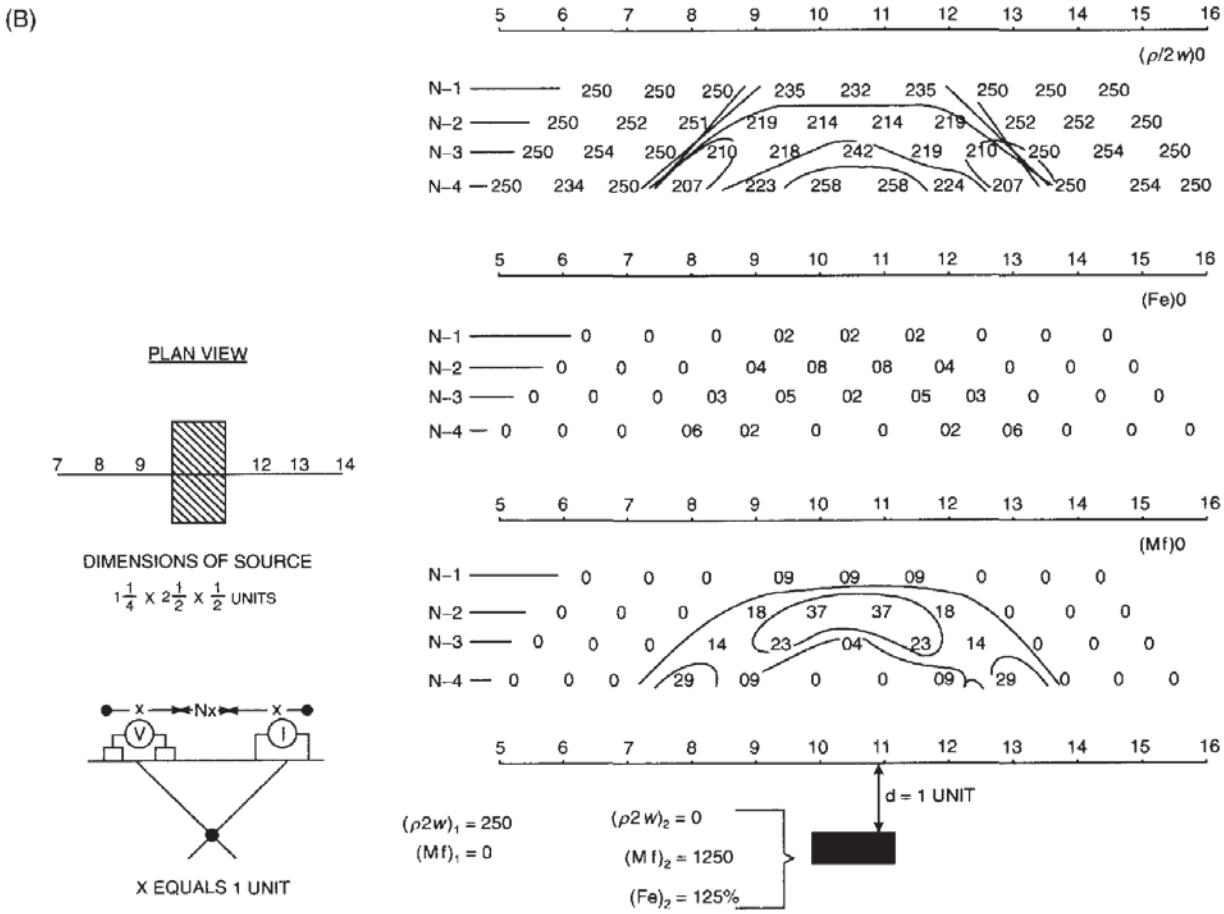
(B)
5 6 7 8 9 10 11 12 13 14 15 16
(ρ/2w)0
N–1 250 250 250 235 232 235 250 250 250
N–2 250 252 251 219 214 214 219 252 252 250
N–3 250 254 250 210 218 242 219 210 250 254 250
N–4 250 234 250 207 223 258 258 224 207 250 254 250
(Fe)0
N–1 0 0 0 02 02 02 0 0 0
N–2 0 0 0 04 08 08 04 0 0 0
N–3 0 0 0 03 05 02 05 03 0 0 0
N–4 0 0 0 06 02 0 0 02 06 0 0 0
(Mf)0
N–1 0 0 0 09 09 09 0 0 0
N–2 0 0 0 18 37 37 18 0 0 0
N–3 0 0 0 14 23 04 23 14 0 0 0
N–4 0 0 0 29 09 0 0 09 29 0 0 0
PLAN VIEW
7 8 9 12 13 14
DIMENSIONS OF SOURCE
1 1/4 X 2 1/2 X 1/2 UNITS
x Nx x
V I
X EQUALS 1 UNIT
(ρ2w)1 = 250
(Mf)1 = 0
(ρ2w)2 = 0
(Mf)2 = 1250
(Fe)2 = 125%
d = 1 UNIT

The apparent resistivity data over the horizontal rectangular block exhibit two 'lows' which correspond to end-effects of the block. Note also the lozenge shape anomaly 'high' in the apparent metal factor over the block model. From these two sets of data, the apparent

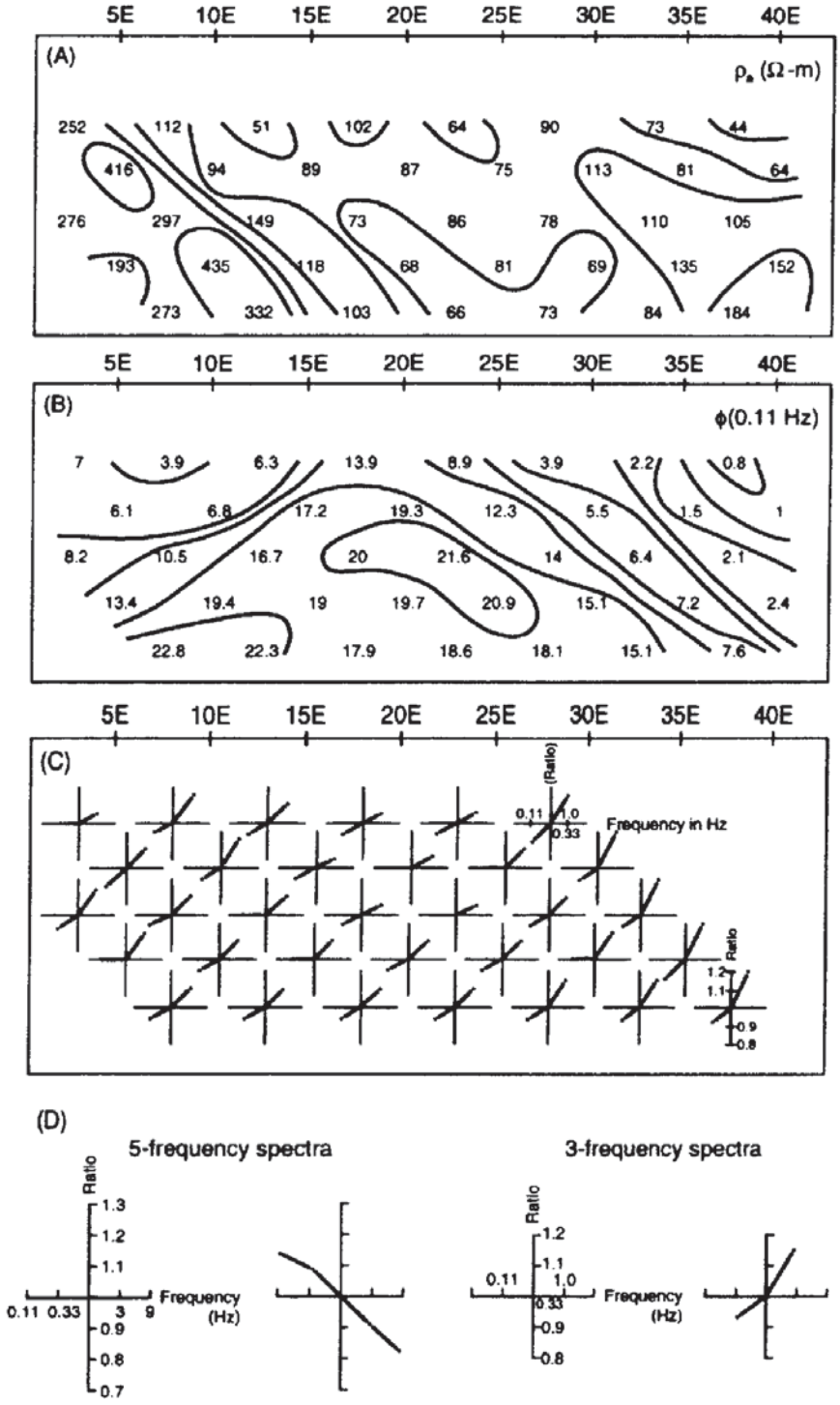

Figure 9.17 (*opposite*) Two model experiments to illustrate the apparent resistivity, frequency effect and metal factor over (A) a thin vertical prism, and (B) a horizontal rectangular block. From Hallof (1967), by permission

Figure 9.18 (*left*) Three forms of pseudo-section display of spectral IP data: (A) apparent resistivity at 1 Hz; (B) phase angle at 0.11 Hz; and (C) ratio of spectral parameters at three frequencies. From Hallof (1982), by permission. (D) Details of each plotting point, showing that the data are normalised to the mid-frequency value which always plots at 1,1 on the graphs (where the two axes cross)

frequency effect is less sensitive to the model and less diagnostic than the apparent metal factor.

Another form of display is the use of three-frequency spectra which are plotted on a modified form of a pseudo-section (Figure 9.18). Spectral IP parameters measured at up to five frequencies, for example 0.11, 0.33, 1.0, 3.0 and 9.0 Hz, are abstracted from the total frequency spectrum and normalised with respect to the value at mid-frequency (i.e. ratio = 1.0); i.e. for five frequencies the parameters are normalised to the value at 1.0 Hz; for three frequencies (0.11–1.0 Hz), they are normalised to the value at 0.33 Hz. The normalised values are then plotted against the frequency (Hallof and Pelton 1981; Hallof 1982) (Figure 9.18D). The shape of the graph at each plotting position can be categorised into 'concave-up' and 'concave-down' (Fraser *et al.* 1964) or into specific and recognisable groupings based on the slope of the graph (Zonge and Wynn 1975; Hallof and Pelton 1981).

The most substantive development of both the display and interpretation of spectal IP is in the computer modelling of observed values of magnitude and phase according to Cole–Cole relaxation models. These permit the recognition and subsequent removal of inductive coupling from the spectra; and in the course of this, the four key IP parameters (ρ_0, M, τ and c) which define the IP response can be determined very accurately. An example of a spectral IP amplitude–phase diagram is given in Figure 9.19. It can be seen that

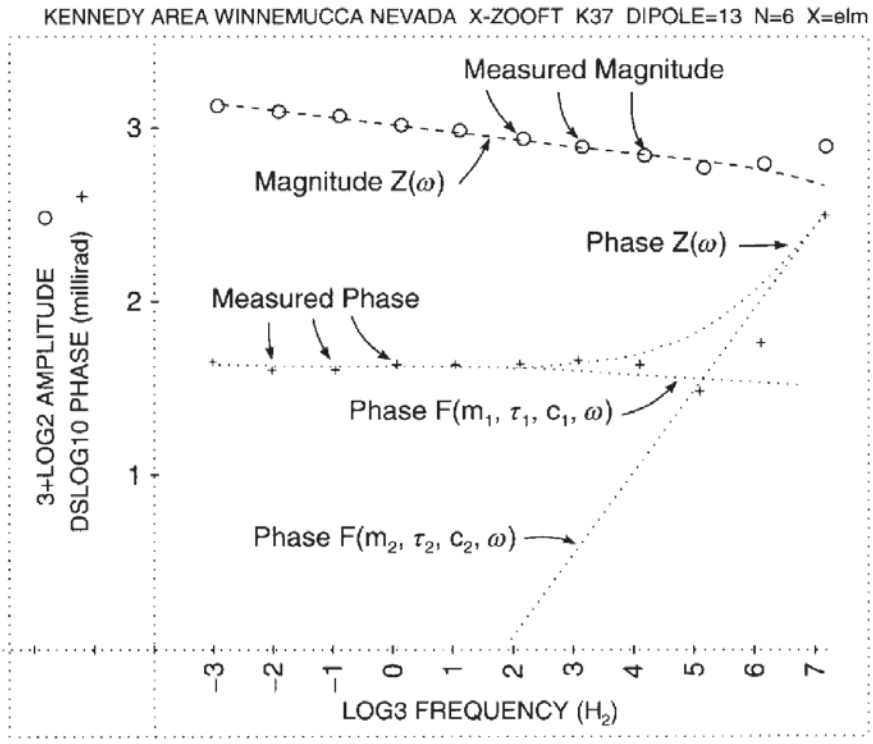

Figure 9.19 Example of a spectral IP amplitude–phase diagram. The steep gradient at high frequencies is due to inductive coupling (dispersion 1) while the data at lower frequencies with almost flat graphs (dispersion 2) can be inverted to give the electrical parameters of the ground. From Hallof 1982), by permission

at low frequencies the inductive coupling has little effect, whereas at high frequencies it becomes dominant.

9.4 APPLICATIONS AND CASE HISTORIES

9.4.1 Base metal exploration

A good example is the IP response over a disseminated copper-ore zone known as the Copper Mountain Orebody in Gaspe Area, Quebec, Canada (Figure 9.20). The orebody has been very well defined by many boreholes and the mineralisation has been evaluated as an average 4% metallic mineralisation comprising both pyrite and chalcopyrite. The increasing thickness of weathering towards the south is picked out by lower apparent resistivities. Low apparent resistivities, high apparent frequency effect and high apparent metal factor all coincide on $n = 3$ and 4 at locations between 46 and 49N, which also correlates with known sulphide mineralisation.

The IP method can produce valuable information about more massive types of mineralisation in cases where electromagnetic

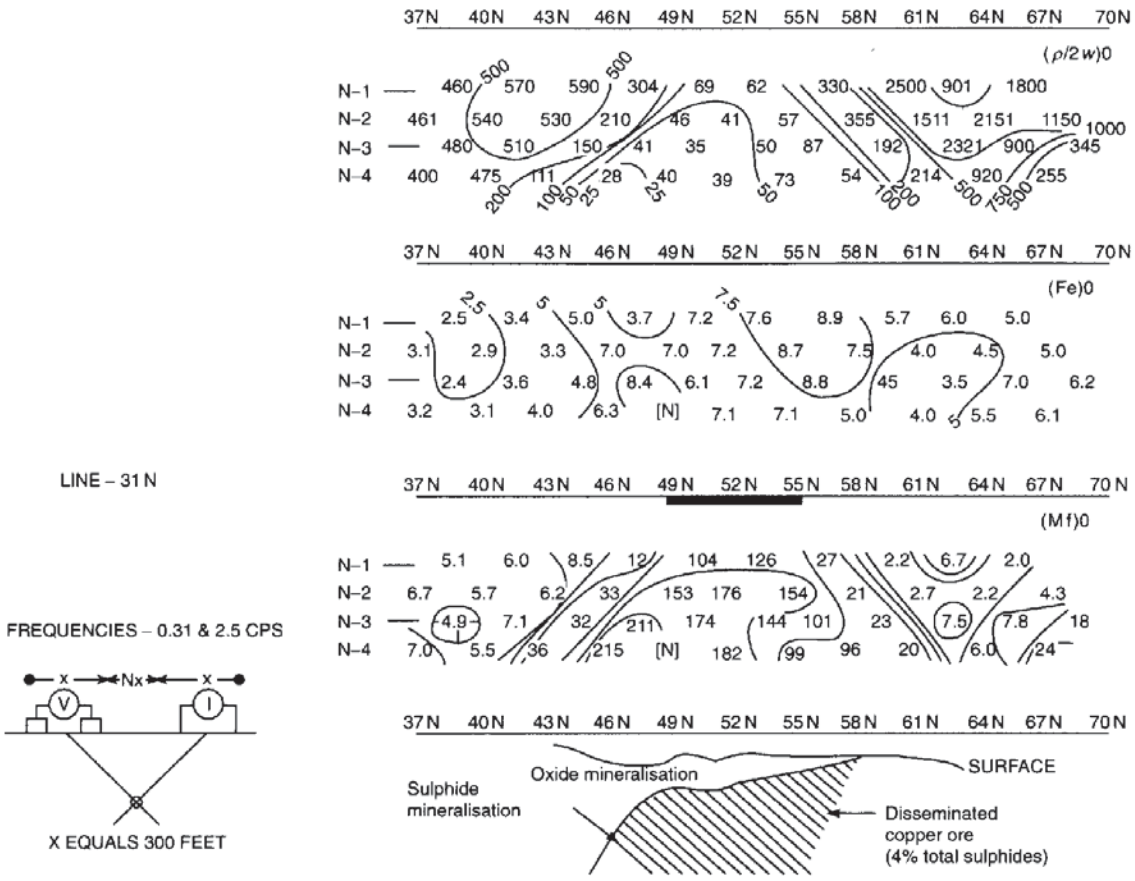

Figure 9.20 Example of induced polarisation data for the Copper Mountain area, Gaspe, Quebec in Canada. From Hallof (1967), by permission

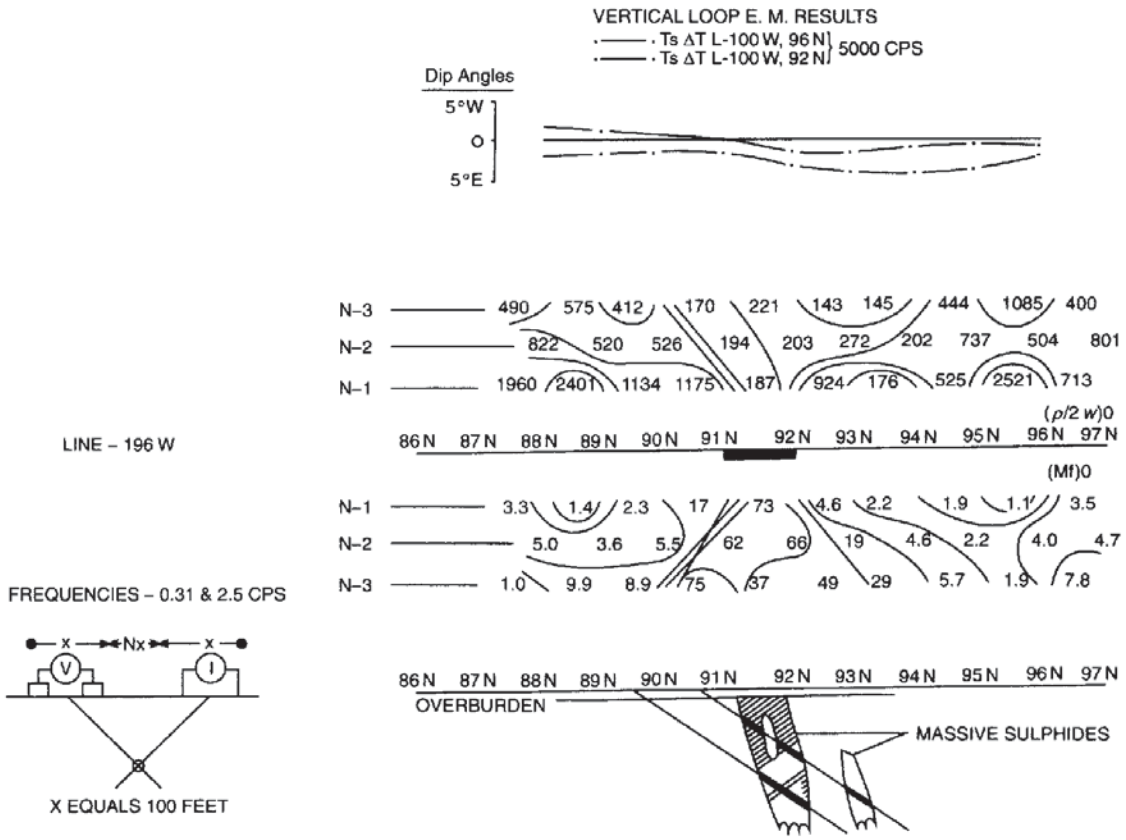

Figure 9.21 Apparent resistivity and apparent metal factor data over a massive sulphide orebody at the Heath Steele Property, Newcastle, New Brunswick, compared with vertical loop EM data which show very poor resolution in contrast with the IP data. From Hallof (1967), by permission

surveying fails. This is due to the mineralisation occurring in veinlets, which do not permit the formation of strong eddy currents in response to an induced electromagnetic field, rather than forming a totally massive orebody. One example of this is for Heath Steele Property, New Brunswick. IP data (apparent resistivity and apparent metal factor) and vertical loop EM data are presented in Figure 9.21, in which it is clear that the EM response is very weak in contrast to IP. The characteristic inverted V shape can be seen in the apparent metal factor data, indicating that the mineralisation is in near-vertical structures, as indicated by subsequent drilling.

Recent case histories of the application of spectral IP in the investigation of six Proterozoic sulphide, oxide and graphitic gneiss deposits in Finland have been described by Vanhala and Peltoniemi (1992). They found that in deposits with large differences in texture, such as graphitic gneiss and coarse-grained disseminated sulphide, could be separated on the basis of their diagnostic phase-spectra constants. They also found a good correlation between the observed grain size (from thin sections) and the grain size calculated from the apparent, field-survey phase spectra in the case of homogeneous disseminated textures.

9.4.2 Geothermal surveys

Geothermal sources often have high fluid mobility within circulating groundwater. This gives rise to low resistivities which can be detected using IP methods. The results on an IP survey over a possible geothermal field in Kenya are shown in Figure 9.22 (Hallof and Pelton 1981), which illustrates low apparent resistivity values for $n = 5$ and 6 between locations 14 and 17. Computer analysis of these data produced a geologically plausible model of a poorly defined but major conductor at a depth of about 350–400 m and a width of about 250 m. Although the survey did not delineate the possible geothermal centre absolutely, it did provide a constrained target for further, more detailed, investigations.

Zohdy *et al.* (1973) have described a combined resistivity, self-potential and induced polarisation survey over a vapour-dominated geothermal field in the Yellowstone National Park, Wyoming, USA (Figure 9.23). The broad SP anomaly is caused by water upwelling (as

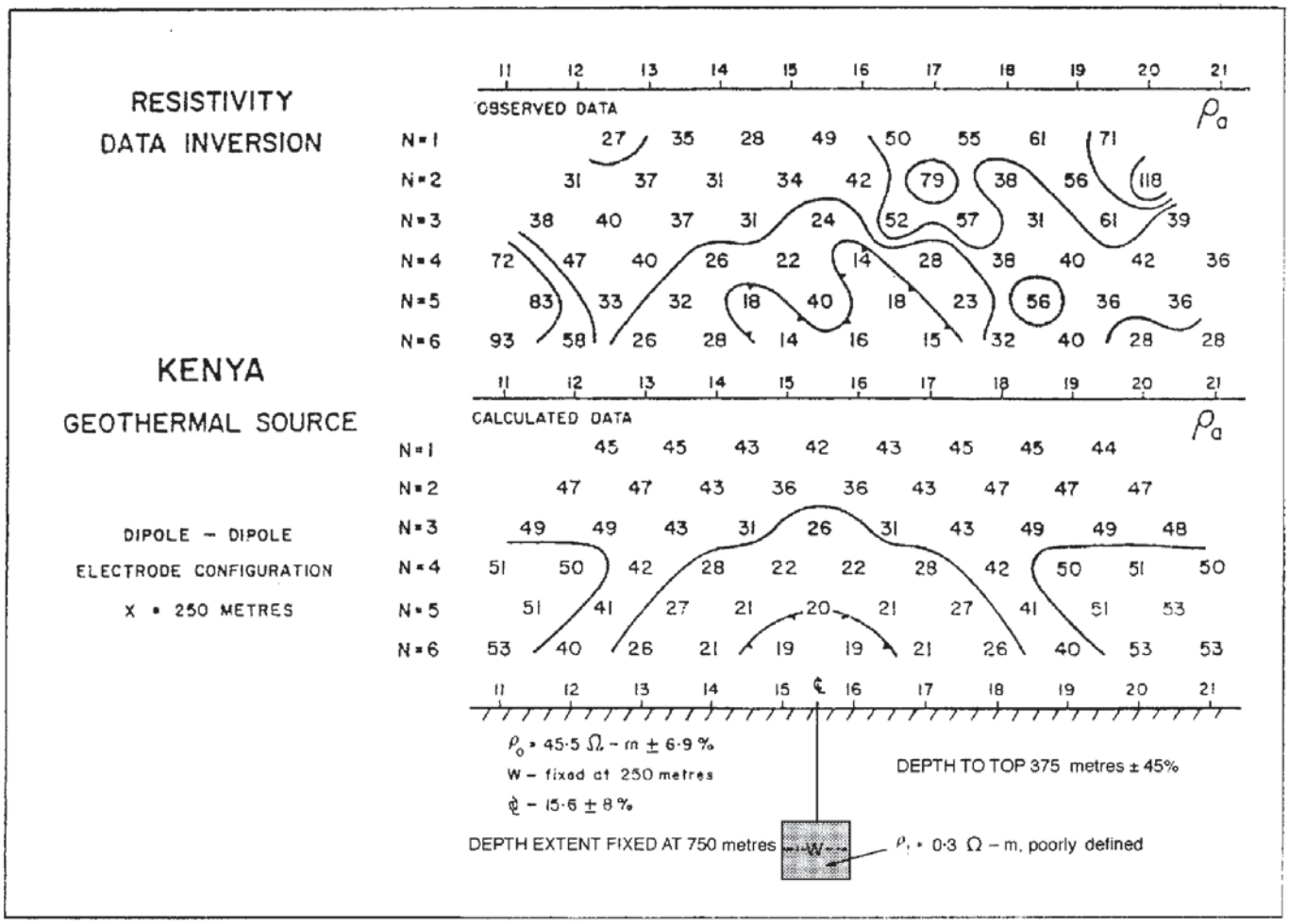

Figure 9.22 Observed and calculated apparent resistivity data obtained during IP surveys of low-resistivity (0.3 Ω m) geothermal source in Kenya. From Hallof and Pelton (1981), by permission

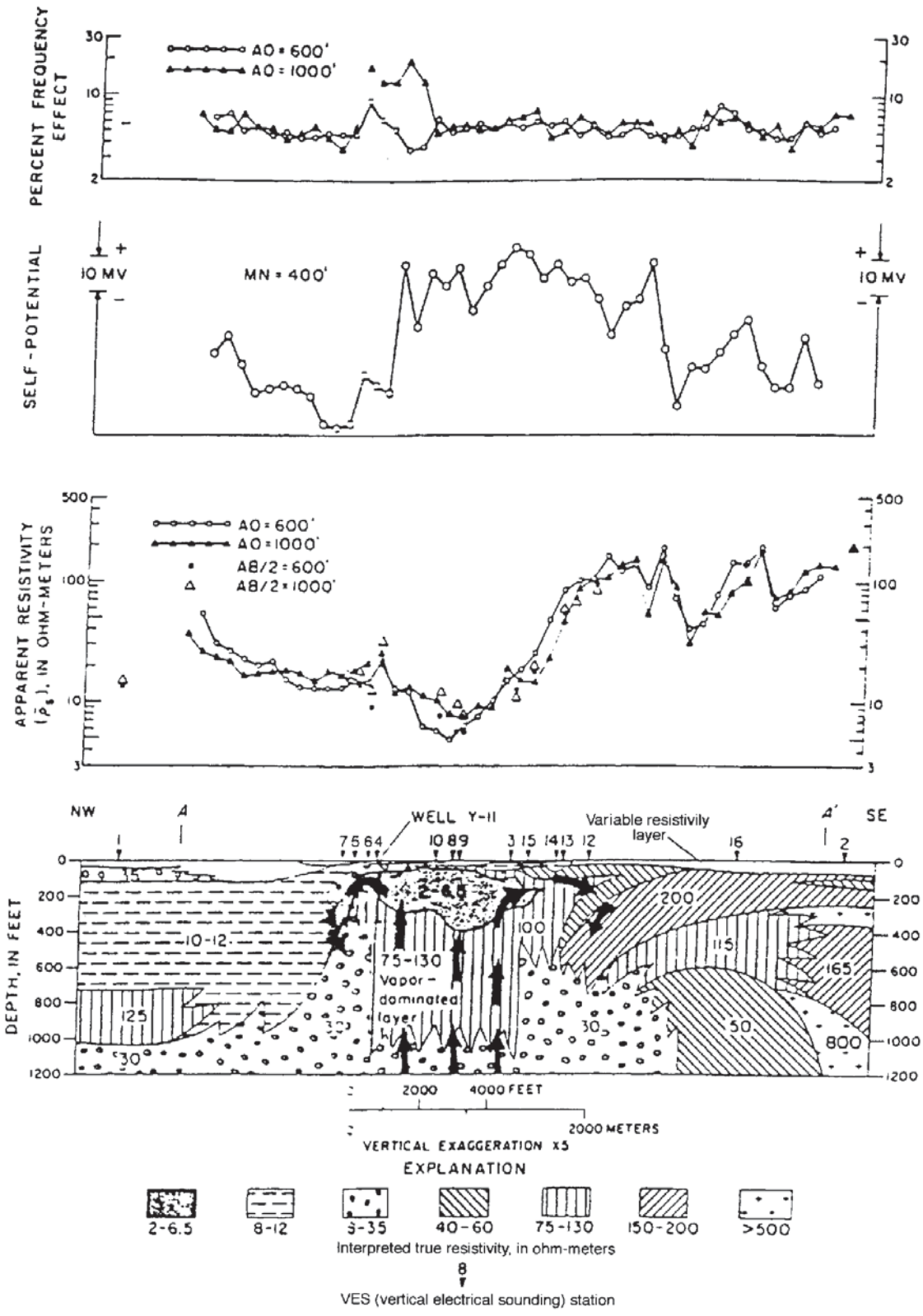
PERCENT FREQUENCY EFFECT
AO = 600'
AO = 1000'
SELF-POTENTIAL
10 MV
MN = 400'
APPARENT RESISTIVITY (ρ_a), IN OHM-METERS
AO = 600'
AO = 1000'
AB/2 = 600'
AB/2 = 1000'
NW
A
WELL Y-11
Variable resistivity layer
A'
SE
DEPTH, IN FEET
75-130
Vapor-dominated layer
2000 4000 FEET
2000 METERS
VERTICAL EXAGGERATION X5
EXPLANATION
2-6.5
8-12
3-35
40-60
75-130
150-200
>500
Interpreted true resistivity, in ohm-meters
VES (vertical electrical sounding) station

indicated by the arrows in the bottom panel of the figure), and continues as far as it does to the south-east because the groundwater flows laterally until it enters more permeable material, at which point it can then descend. The resistivity profiles reflect the general distribution of formations, with those to the north-west having lower true resistivities (10–130 Ω m) than those to the south-east (> 130 Ω m). The percentage-frequency-effect profile has a significant background of around 5%, which has been attributed to the presence of clayey materials and pyrite in the near-surface materials. The IP anomaly which is particularly prominent with $AO \approx 300$ m is due to an increase in disseminated pyrite deposited by circulating thermal waters as indicated from borehole data in the area.

Figure 9.23 (*opposite*) Percentage frequency effect and apparent resistivity data across a vapour-dominated geothermal system in the Yellowstone National Park (interpreted geological cross-section shown in the lowest panel) compared with a self-potential profile across the same feature. From Zohdy *et al.* (1973), by permission

9.4.3 Groundwater investigations

Vacquier *et al.* (1957), who were the first to use induced polarisation for hydrogeological investigations, have described two useful case histories. The first is for a site near Carrizozo, New Mexico, in a valley bounded to the south-east by the Sierra Blanca which comprise volcanic rocks from which potable water is derived. To the north and west, Cretaceous sediments of the Tularosa Valley contaminate the groundwater with chlorides and gypsum making it unusable.

Figure 9.24A shows a map of IP values 10 s after current shutoff; the contours are orientated approximately north–south and mirror the existing drainage pattern the boundaries of which correlate with contours of 2 mV/V in the east and 3 mV/V in the west. An irrigation well IR-1 produces about 4500 litres/minute of relatively poor quality water; hence the low IP overvoltage (≈3 mV/V). The closure with a value of 6 mV/V (L-1) was subsequently drilled and produced about 450 litres/minute of better quality water. The map shown in Figure 9.24B shows contours of the ratio of IP values 5 s after current shutoff to those after 10 s. Vacquier and colleagues interpreted these contours as highlighting a buried channel, with the higher ratios being associated with finer grained material.

Ogilvy and Kuzmina (1972) carried out a laboratory scale model experiment to examine the effectiveness of time-domain IP measurements in locating groundwater accumulations in sandy–clayey overburden. While standard constant-separation traversing over a hemispherical freshwater lens produced a broad apparent resistivity anomaly, the IP polarisability anomaly was both narrow and steep-sided (Figure 9.25A); a result which had also been obtained by Vacquier *et al.* (1957, p. 684). However, for a model with the same dimensions and geometry, but with a saline water lens, both the apparent resistivity and IP chargeability anomalies were broad in contrast with the ratio of IP overvoltages after 0.5 s and 5 s after current shutoff (Figure 9.25B).

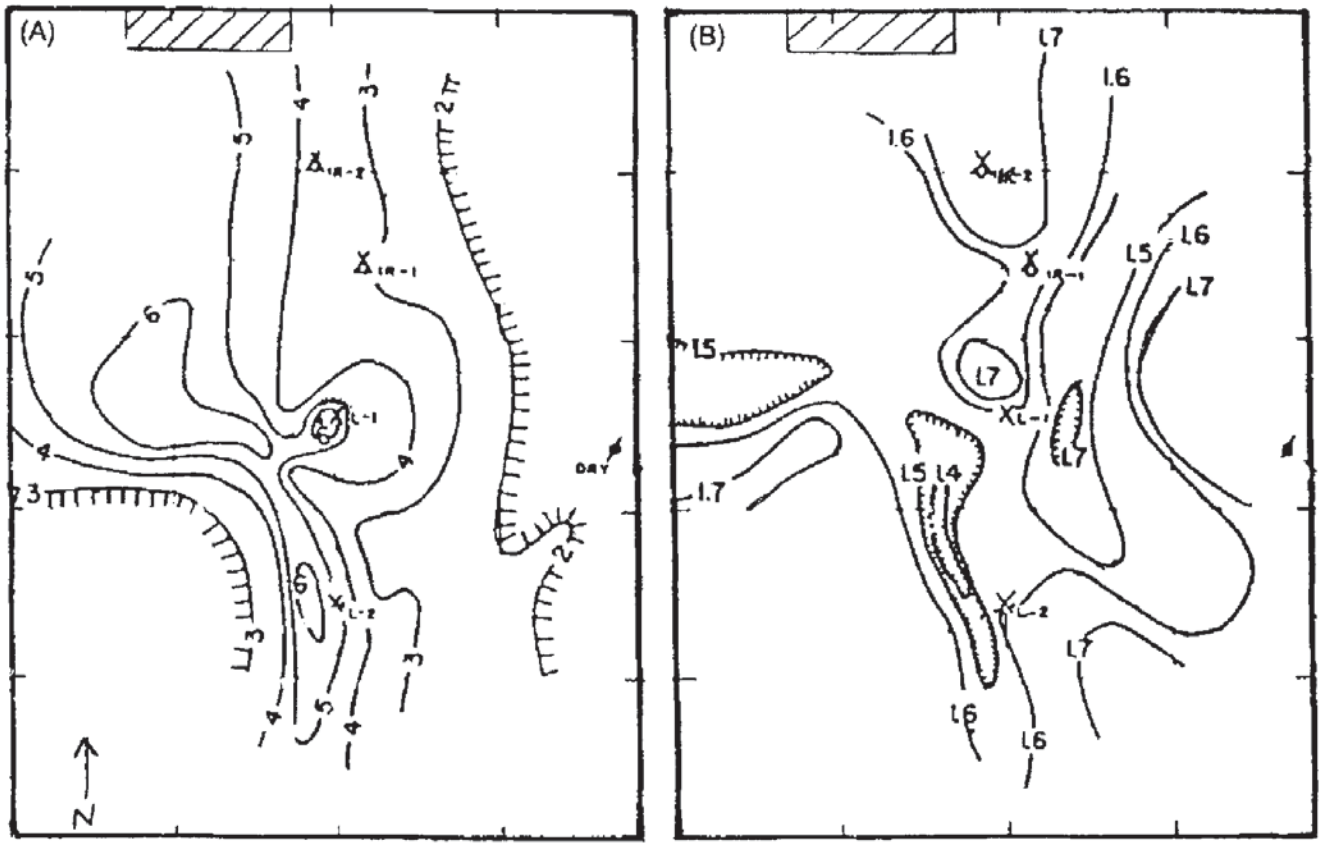

Figure 9.24 Maps of: (A) induced polarisation overvoltage after 10 s (contours at 1 mV/V intervals); and (B) the ratio of IP data after 5 s and 10 s after current switchoff, over a buried valley aquifer near Carrizozo, New Mexico, USA. The well sunk at L-1 produced about 450 litres/minute of potable water. From Vacquier *et al.* (1957), by permission

The examples from Vacquier and colleagues and from Ogilvy and Kuzmina demonstrate that for time-domain IP, maps of the ratio of the overvoltage for two different times can provide a sharper resolution of sub-surface water bodies than maps of the overvoltage for single cutoff times. While the IP method can provide a useful interpretation of groundwater bodies, the field method is less practical than modern electromagnetic induction methods, and this may account for the paucity of recent examples of the use of IP in groundwater investigations.

9.4.4 Environmental applications

Since the early 1980s, interest has been expressed in the possibility of using IP in the investigation of contaminated sites. Olhoeft (1985), for example, investigated the IP characteristics of rocks contaminated with organic pollutants. Organic chemicals can react with clay minerals so that the IP response of the clay mineral–electrolyte mixture changes. This work has been extended by Soininen and Vanhala (e.g. 1992), for example, who have investigated laboratory samples of glacial clays contaminated with ethylene glycol using spectral IP methods. They have found that both the phase and resistivity spectra

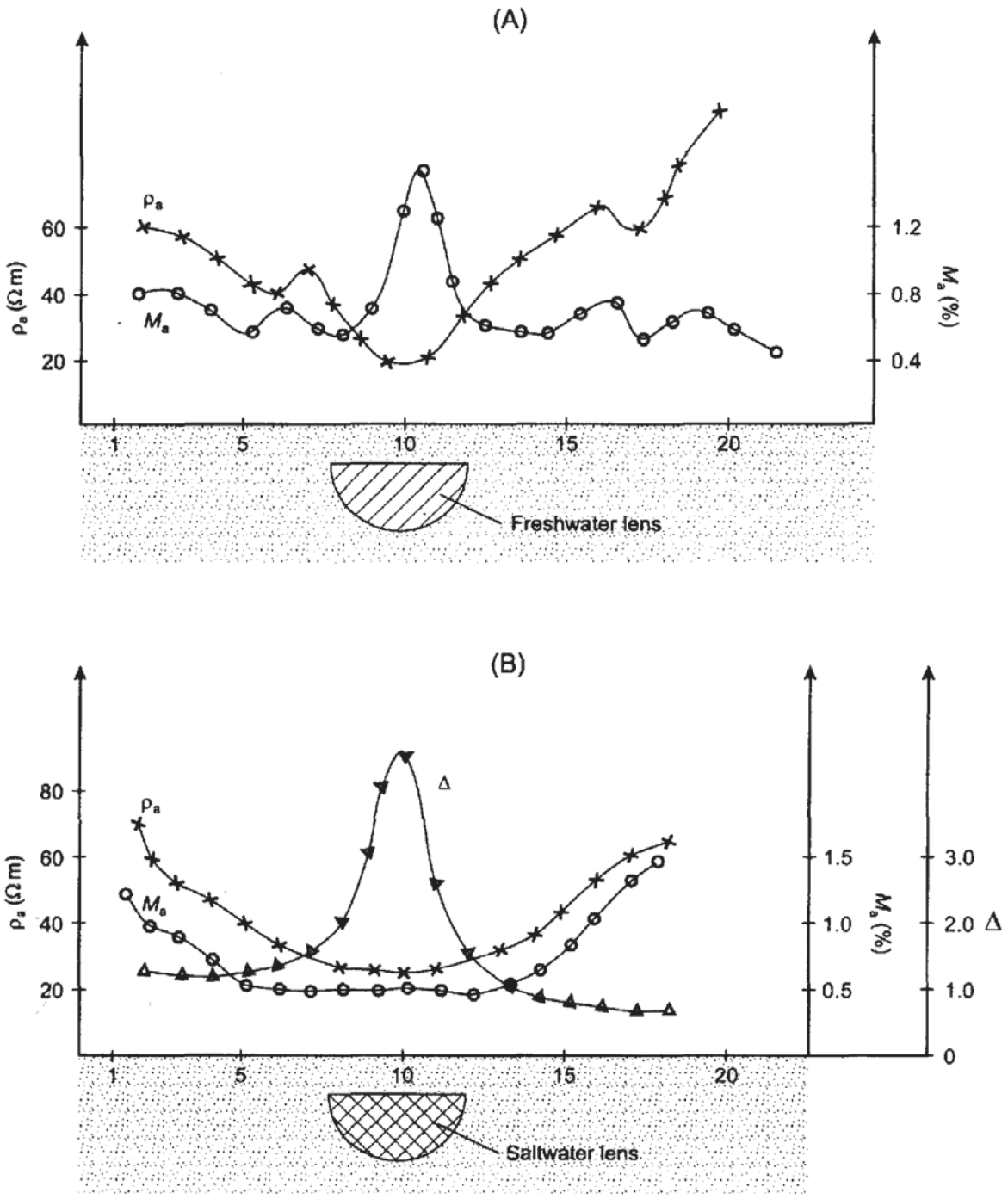

Figure 9.25 Scale model experimental results of apparent resistivity, chargeability, and ratio (Δ) of overvoltage measured after 0.5 minutes and 5 minutes after current switch obtained across a buried hemispherical lens of (A) freshwater and (B) saltwater. After. Ogilvy and Kuzmina (1972), by permission

(as functions of frequency) of contaminated samples differ significantly from those of uncontaminated samples. Whether this technique can be extended to achieve a fully commercial field survey technique has yet to be demonstrated.

Cahyna *et al.* (1990) have presented a case history where the field use of standard IP, in conjunction with appropriate laboratory measurements, was instrumental in mapping out an area seriously

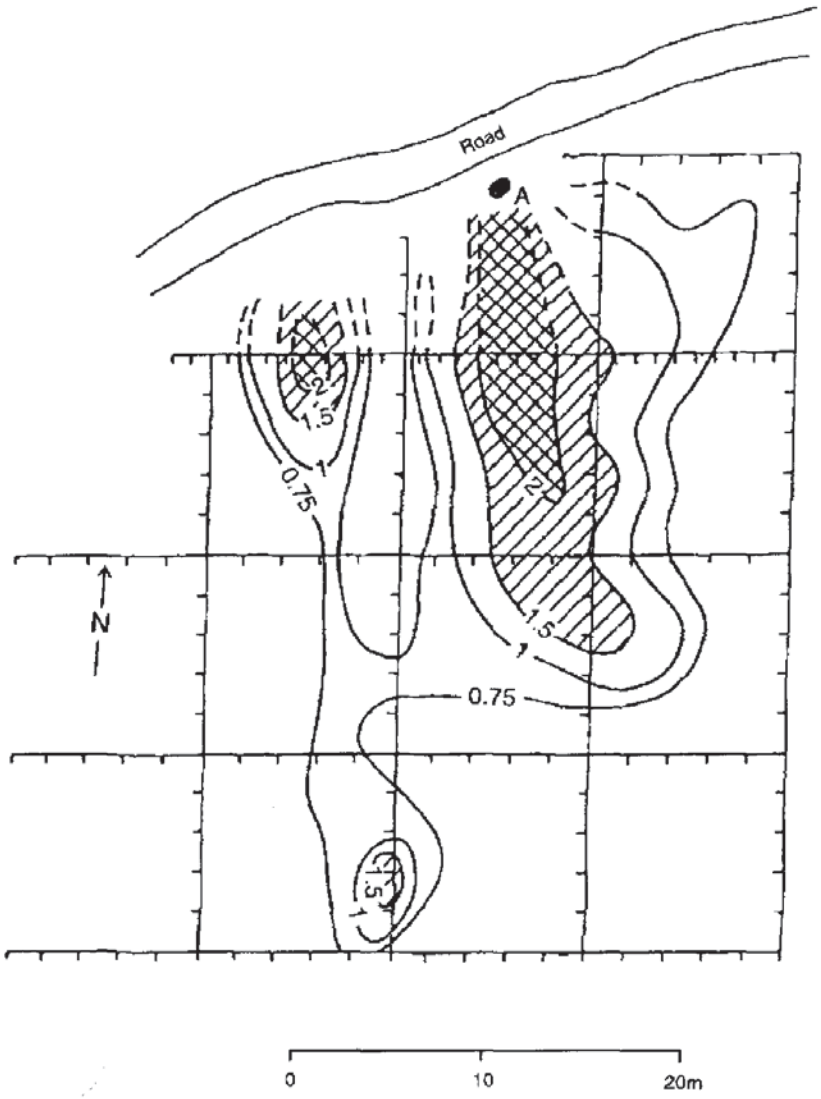

Figure 9.26 Chargeability map over a site contaminated with cyanide complexes. The location of a known outcrop of slag is indicated at A. Contours are in percentage chargeability. Shaded areas indicate the interpreted extent of contaminated land. From Cahyna *et al.* (1990), by permission

contaminated with cyanide complexes which originated from slag-type material from former plating works. They used both conventional resistivity sounding (using the Schlumberger array) and symmetrical resistivity profiling with IP (called SRP-IP by the authors). The resistivity survey failed to detect the contamination even though measured directly over a known slag deposit. In contrast, the SRP-IP survey, which was used to measure chargeability, was used successfully to identify not only the limit of the known slag, but also to detect a second and previously unknown area of contamination. A map of the SRP-IP chargeability was produced (Figure 9.26) on which the centres of contamination and the affected areas around them are clearly evident.